LBNL-41857
Preprint

ERNEST ORLANDO LAWRENCE
BERKELEY NATIONAL LABORATORY

Semi-Analytical Solutions for Parameter Estimation in Diffusion Cell Experiments

George J. Moridis

Earth Sciences Division

June 1998

Submitted to
Water Resources Research

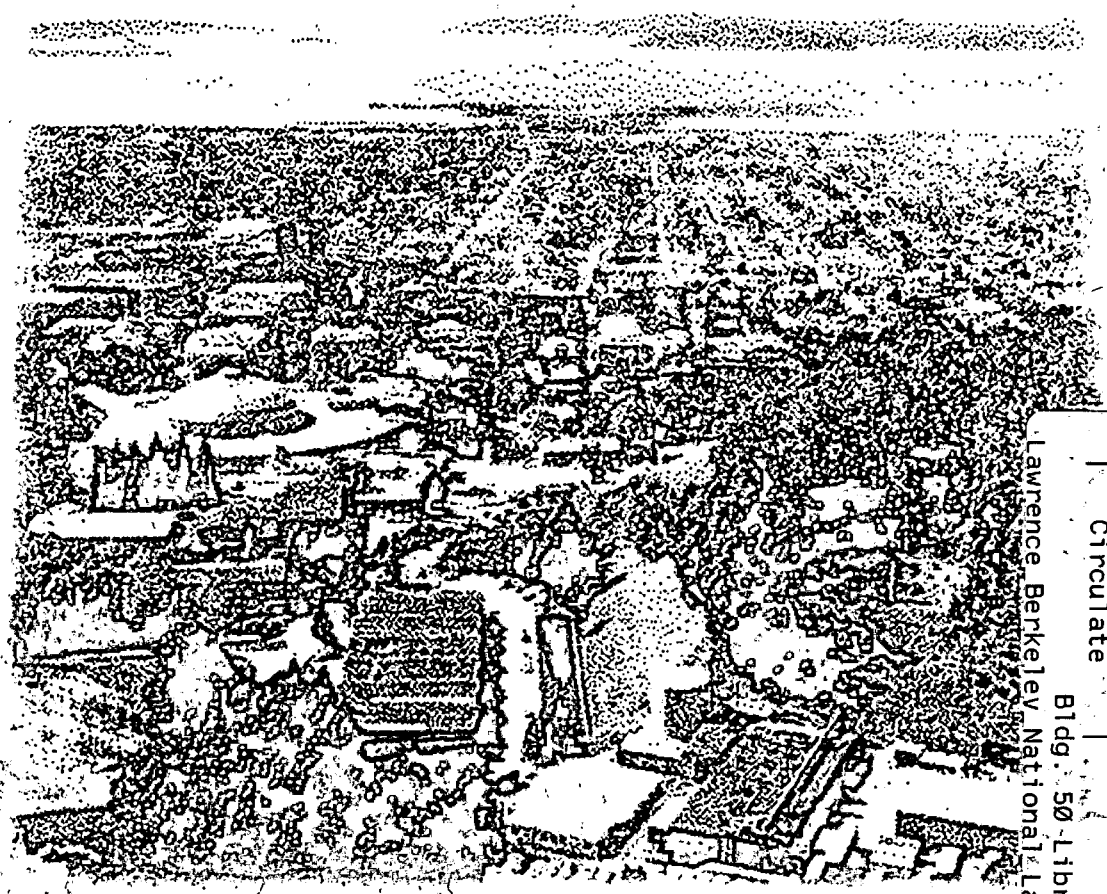

REFERENCE COPY
Does Not
Circulate
Bldg. 50-Library - Ref.
Lawrence Berkeley National Laboratory
LBNL-41857
Copy 1

DISCLAIMER

This document was prepared as an account of work sponsored by the United States Government. While this document is believed to contain correct information, neither the United States Government nor any agency thereof, nor the Regents of the University of California, nor any of their employees, makes any warranty, express or implied, or assumes any legal responsibility for the accuracy, completeness, or usefulness of any information, apparatus, product, or process disclosed, or represents that its use would not infringe privately owned rights. Reference herein to any specific commercial product, process, or service by its trade name, trademark, manufacturer, or otherwise, does not necessarily constitute or imply its endorsement, recommendation, or favoring by the United States Government or any agency thereof, or the Regents of the University of California. The views and opinions of authors expressed herein do not necessarily state or reflect those of the United States Government or any agency thereof or the Regents of the University of California.

LBNL-41857

SEMIANALYTICAL SOLUTIONS FOR PARAMETER ESTIMATION IN DIFFUSION CELL EXPERIMENTS

George J. Moridis

Earth Sciences Division
Lawrence Berkeley National Laboratory
Berkeley, CA 94720

June 1998

This work was supported by the U.S. Department of Energy, Office of Environmental Management, Office of Technology Development, Subsurface Contamination Focus Area, under Contract No. DE-AC03-76SF00098.

Semianalytical Solutions for Parameter Estimation in Diffusion Cell Experiments

George J. Moridis
Earth Sciences Division, Lawrence Berkeley National Laboratory, University of California, Berkeley, California

Abstract. In this paper, semianalytical solutions to the diffusion problem are developed under the conditions of diffusion cell experiments, which involve finite liquid volumes and temporally variable concentrations in the upstream and downstream reservoirs. These solutions account for diffusion in the pores, surface diffusion, mass transfer between the mobile and immobile water fractions, linear sorption (equilibrium, kinetic or irreversible), and radioactive decay. Fully analytical solutions for both through-diffusion and reservoir-depletion studies are obtained in the Laplace space, which are subsequently numerically inverted to provide the solution in time. The effects of the various diffusion, sorption and geometric parameters on the solutions are investigated, and scoping calculations for a realistic problem of radionuclide fate and transport are presented. Two numerical inversion schemes are evaluated, and are shown to produce comparable results. The semianalytical solutions are coupled with a history-matching algorithm, and diffusion and sorption parameters are estimated using experimental data. The use of the semianalytical solutions is shown to have significant advantages over the conventional graphical approach because (a) it is not based on the often invalid assumption of constant upstream and negligible downstream concentrations, and (b) it doubles the amount of data from which to extract the pertinent diffusion and sorption parameters.

1. Introduction

The deep disposal or isolation of contaminants by using natural or engineered barriers necessitates an understanding of their fate and transport in the subsurface. This is particularly important in the case of radionuclide storage and the performance of radioactive-waste repositories. Diffusion through, and sorption onto geological materials are important mechanisms of transport and immobilization, and an accurate evaluation of the pertinent parameters is of critical importance.

Diffusion experiments represent a well established technique for the determination of the transport properties of conservative and non-conservative tracers. *Lever* [1986] and *Shackelford* [1991] presented thorough reviews of most diffusion techniques, and discussed their capabilities and limitations. The majority of studies involve two basic diffusion cell designs: the through-diffusion cell, or the reservoir-depletion/in-diffusion cell. A schematic of these two types of cells is shown in Figure 1. Through-diffusion cells have been used extensively for the study of geologic materials [*Bradbury et al.*, 1982; 1986; *Skagius and Neretnieks*, 1986*a*; 1988; *Kirchner et al.*, 1996; *McKinley and Swaminathan*, 1996; *Wen et al.*, 1997], while reservoir-depletion/in-diffusion cells are commonly used in the analysis of the diffusion of polymers [*McKinley and Swaminathan*, 1996].

No analytical solutions to the problem of diffusion and sorption under the conditions of diffusion cell experiments (i.e., finite liquid volumes and temporally variable concentrations in the upstream and downstream reservoirs) are currently available [*Kirchner et al.*, 1996]. Numerical solutions are commonly used to analyze the experimental data for parameter estimation [*Skagius and Neretnieks*, 1986*a*; *Kirchner et al.*, 1996; *Wen et al.*, 1997]. The majority of the through-diffusion analyses, however, are conducted using the time-lag method, which is based on the approximate analytical solution of *Crank* [1975], as adapted by *Skagius and Neretnieks* [1986*a*]. This solution is further discussed in Section

5.1.1.

The time-lag method assumes a linear equilibrium model, and is valid if (1) the concentration C_U of the upstream reservoir remains constant over time, (2) the concentration C_D of the downstream reservoir is sufficiently low to be negligible compared to C_U, (3) the diffusion coefficient is constant, and (4) diffusion is the only transport mechanism, i.e., there is no advection [*Skagius and Neretnieks*, 1986*b*]. Condition (3) is usually valid, while condition (4) can be achieved with careful experimental preparation. Regarding conditions (1) and (2), these may be good approximations in the initial stages of the study, but their validity deteriorates as time advances and may lead to erroneous diffusion and sorption parameters, especially in the case of strong sorption. To overcome this shortcoming, current laboratory practices involve diffusion cells with large upstream and downstream reservoirs, while data analysis is restricted to the early portion of the data. An alternative approach, which involves maintaining constant concentration by replenishing the depleted species in the upstream reservoir, is cumbersome and requires special equipment.

Additionally, the time-lag method assumes a quasi-steady diffusion after an initial transient period. Parameter estimation is based on the slope and intercept of the C_U vs. time curve, which are determined using a semi-empirical (graphical) method involving only the apparent linear portion of the data set [*Skagius and Neretnieks*, 1986*a*; *McKinley and Swaminathan*, 1996]. Thus, the conventional approach uses information from only the downstream reservoir, and only a portion of the data which is early and linear. The often subjective nature of parameter estimation can lead to substantial errors and ambiguities.

In this paper, general semianalytical solutions to the diffusion problem are developed under the conditions of diffusion cell experiments. These include finite liquid volumes and temporally variable concentrations in the upstream and downstream reservoirs, and involve practically no simplifying assumptions. The solutions account for diffusion in the pores, surface diffusion, mass transfer between the mobile and immobile water fractions,

linear sorption (equilibrium, kinetic or irreversible), and radioactive decay. Fully analytical solutions for both through-diffusion and reservoir-depletion studies are obtained in the Laplace space, which are subsequently numerically inverted to provide the solution in time. The semianalytical solutions are shown to have significant advantages over the conventional graphical approach because (a) they are not based on the often invalid assumption of constant upstream and negligible downstream concentrations, and (b) can double the amount of data from which to extract the pertinent diffusion and sorption parameters.

2. Governing Equations

2.1. The Diffusion Equation in Through-Diffusion Studies

The 1-D solute transport through the porous medium (PM) in a diffusion cell such as the one shown in Figure 1a is described by the equation

$$\begin{aligned} D_m \frac{\partial^2 C}{\partial x^2} + D_i \frac{\partial^2 C_i}{\partial x^2} + \phi D_F \frac{\partial^2 F}{\partial x^2} \\ = \phi_c \frac{\partial C}{\partial t} + (\phi - \phi_c) \frac{\partial C_i}{\partial t} + (1-\phi)\rho \frac{\partial F}{\partial t} \\ + \phi_c \lambda C + (\phi - \phi_c)\lambda C_i + (1-\phi)\rho\lambda F, \end{aligned} \tag{1}$$

where

C species concentration in the mobile pore water $[ML^{-3}]$;

D_m intrinsic diffusion coefficient for the mobile pore water $[L^2T^{-1}]$;

C_i species concentration in the immobile pore water $[ML^{-3}]$;

D_i intrinsic diffusion coefficient in the immobile pore water $[L^2T^{-1}]$;

F relative concentration of the adsorbed mass [*dimensionless*];

D_F apparent surface diffusion coefficient $[L^{-1}MT^{-1}]$;

ρ PM grain density $[ML^{-3}]$;

ϕ total PM porosity [*dimensionless*];

ϕ_c kinematic porosity [*dimensionless*];

λ = $\ln 2/T_{1/2}$, radioactive decay constant [T^{-1}];

$T_{1/2}$ half-life of radioactive species [T];

x length coordinate in the diffusion equation [L];

t time [T].

The three terms on the left-hand side of equation (1) describe diffusion in the mobile pore water [*Skagius and Neretnieks*, 1988], through the immobile thin *film* in the immediate vicinity of the PM grains [*de Marsily*, 1986], and surface diffusion [*Jahnke and Radke*, 1987; *Skagius and Neretnieks*, 1988; *Cook*, 1989; *Berry and Bond*, 1992], respectively. The first and second sets of three terms each on the right-hand side of equation (1) describe the dissolved species accumulation and radioactive decay in the pore water, in the immobile fraction, and on the PM grains due to sorption, respectively. The kinematic porosity ϕ_c is defined as the portion of the porosity corresponding to the mobile fraction of the fluid phase [*de Marsily*, 1986], and can be approximated by

$$\phi_c = \phi\,(1 - S_r), \tag{2}$$

where S_r is the irreducible water saturation, which can be obtained from the *van Genuchten* [1980] capillary pressure curve of the PM.

From *Oldenburg and Pruess* [1995] and *Skagius and Neretnieks* [1986*a*]

$$D_m = \tau_p\,\phi_c\,D_0 = \tau_p\,\phi\,(1 - S_r)\,D_0, \tag{3}$$

where τ_p is the tortuosity factor of the pore paths [*dimensionless*], and D_0 is the molecular diffusion coefficient of the dissolved species in water [L^2T^{-1}]. Similarly,

$$D_i = \tau_i\,(\phi - \phi_c)\,D_0 = \tau_i\,\phi\,S_r\,D_0, \tag{4}$$

where τ_i is the tortuosity factor in the diffusion paths through the immobile fraction [*dimensionless*]. If surface diffusion cannot be neglected [*Jensen and Radke*, 1988], D_F is

given by [*Jahnke*, 1986; *Jahnke and Radke*, 1987]

$$D_F = \tau_s \frac{(1-\phi)}{\phi} \rho D_s, \tag{5}$$

where τ_s is the tortuosity factor of the surface path [*dimensionless*], and D_s is the surface diffusion coefficient [L^2T^{-1}]. For homogeneous PM systems there is theoretical justification [*Cook*, 1989] for the relationship $\tau_s = \frac{2}{3}\tau_p$.

Assuming a linear equilibrium relationship between between C and C_i [*de Marsily*, 1986],

$$C_i = K_i C, \tag{6}$$

where K_i is a mass transfer coefficient [*dimensionless*], equation (1) becomes

$$D_T \frac{\partial^2 C}{\partial x^2} + D_F \frac{\partial^2 F}{\partial x^2} = h \left(\frac{\partial C}{\partial t} + \lambda C \right) + \frac{(1-\phi)}{\phi} \rho \left(\frac{\partial F}{\partial t} + \lambda F \right), \tag{7}$$

where

$$D_T = D_0 \left[\tau_p (1 - S_r) + \delta \tau_i S_r K_i \right] \tag{8}$$

and

$$h = \frac{\phi_c}{\phi} + \frac{\phi - \phi_c}{\phi} K_i = 1 - S_r + S_r K_i . \tag{9}$$

The parameter δ may be either 1 or 0. For $\delta = 0$, diffusion in the immobile water fraction is ignored.

The initial and boundary conditions are

$$C(x=0,t) = C_U(t), \qquad C_U(0) = C_{U0} \neq 0, \tag{10}$$

$$C(x=L,t) = C_D(t), \qquad C_D(0) = 0, \quad \text{and} \quad C(x,t=0) = 0, \tag{11}$$

where L is the length of the PM compartment ([L], see Figure 1a). An additional condition is imposed by the dissolved species mass conservation, i.e.,

$$m_U + m_W + m_S + m_D = m_T \qquad \text{for} \quad t \geq 0, \tag{12}$$

where m_U, m_W, m_S, m_D, and m_T are the species mass $[M]$ in the upstream reservoir, in the pore water of the PM, adsorbed onto the PM grains, in the downstream reservoir, and in the whole system, respectively. It is obvious that

$$m_T = V_U\, C_{U0} \exp(-\lambda t), \tag{13}$$

where V_U is the liquid volume in the upstream reservoir $[L^3]$. For a non-radioactive species, $\lambda = 0$ and $m_T = V_U\, C_{U0}$, i.e., constant over time.

The final boundary condition in through-diffusion studies equates the dissolved species mass in the downstream reservoir with the mass that crosses the $x = L$ boundary, i.e.,

$$\begin{aligned} -\int_0^t A\,\phi\, D_T \left(\frac{\partial C}{\partial x}\right)_{x=L} dt - \int_0^t A\,\phi\, D_F \left(\frac{\partial F}{\partial x}\right)_{x=L} dt \\ = V_D \left(C_D + \lambda \int_0^t C_D\, dt\right), \end{aligned} \tag{14}$$

where V_D is the downstream reservoir volume $[L^3]$, and A is the cross-sectional area of flow $[L^2]$. For non-radioactive species, $\lambda = 0$ and $m_D = V_D\, C_D$. In reservoir-depletion and in-diffusion studies, equation (14) applies with $V_D = 0$, i.e., by setting the right-hand side of the equation equal to zero.

Equation (7), subject to the conditions of equations (10) through (14), is the general equation of diffusion. The only assumption made is that the concentration in the upstream and downstream reservoirs are uniform, i.e., they are well mixed, and there are no spatial concentration gradients in either. This is a valid assumption because the solutions in the reservoirs of diffusion cells are continuously stirred [*McKinley and Swaminathan*, 1996].

2.2. The Sorption Equation

Considering that sorption occurs as the dissolved species diffuses through the immobile water fraction, and assuming that the sorption is linear, instantaneous and reversible (i.e., equilibrium linear sorption), the following relationship applies:

$$F = K_d \, K_i \, C \, , \tag{15}$$

where K_d is the distribution coefficient $[L^3 M^{-1}]$. The validity of this approach is supported by experimental evidence [*de Marsily*, 1986], which suggests that equilibrium is reached in a matter of a few minutes in clayey PMs, i.e., practically instantaneously, given that diffusion experiments routinely last from days to months. Equation (15) is the most general form of the linear sorption equation, and accounts for the effect of mass transfer through the immobile water fraction. If, however, this effect is disregarded, $K_i = 1$ and equation (15) reverts to the more commonly used form of linear sorption.

The linearity of equation (15) allows its combination with the general diffusion equation (7) and with the boundary equation (14), yielding

$$\frac{\partial^2 C}{\partial x^2} = \frac{R^*}{D^*} \left(\frac{\partial C}{\partial t} + \lambda \, C \right) , \tag{16}$$

and

$$-A \, \phi \, D^* \int_0^t \left(\frac{\partial C}{\partial x} \right)_{x=L} dt = V_D \left(C_D + \lambda \int_0^t C_D \, dt \right) ; \tag{17}$$

where the retardation factor R^* and the effective diffusion coefficient D^* are defined by

$$R^* = \underbrace{1 - S_r + S_r \, K_i}_{h} + \underbrace{\frac{1-\phi}{\phi} \, \rho \, K_d \, K_i}_{w} \quad \text{and} \quad D^* = D_T + \tau_s \, w \, D_s . \tag{18}$$

For non-radioactive species, equation (16) applies with $\lambda = 0$.

If sorption is not in equilibrium and its kinetics are linear [*de Marsily*, 1986], the temporal variation of F [*Harada et al.*, 1980; *Pigford et al.*, 1980] is modified to account

for radioactive decay, yielding

$$\frac{\partial F}{\partial t} + \lambda F = k\,(K_d\,K_i\,C\ - F)\,, \tag{19}$$

where k is the kinetic constant of linear chemical adsorption $[T^{-1}]$.

Linear irreversible sorption is decribed by the relationship [*Bear*, 1979]

$$\frac{\partial F}{\partial t} + \lambda F = K_L\,K_i\,C\,, \tag{20}$$

where K_L is a constant $[L^3M^{-1}T^{-1}]$. Equation (20) indicates a solid phase acting as a sink for the dissolved species.

The non-linearity of equations (19) and (20) does not permit substitution in (7), and the equations of diffusion and sorption must be solved simultaneously.

3. The Laplace Space Solutions

3.1. Through-Diffusion With Linear Equilibrium

The Laplace transform of the governing equation (16) results in

$$\frac{\partial^2 \Psi}{\partial x^2} - \frac{R^*}{D^*}\,(s+\lambda)\,\Psi = 0\,, \tag{21}$$

where $\Psi = \mathcal{L}\{C\}$, s is the Laplace space parameter, and $\mathcal{L}\{\}$ denotes the Laplace transform of the term within the brackets. A general solution to equation (21) is

$$\Psi(x) = \alpha \exp(m\,x) + \beta \exp(-m\,x)\ , \tag{22}$$

where

$$m = \sqrt{\frac{R^*}{D^*}\,(s+\lambda)}\,, \tag{23}$$

and α and β are coefficients to be determined. From (22) and the Laplace transform of the boundary conditions (10) and (11),

$$\begin{aligned} \Psi_0 &= \mathcal{L}\{C_U\} = \Psi(x=0,s) = \alpha + \beta \\ \Psi_L &= \mathcal{L}\{C_D\} = \Psi(x=L,s) = \alpha \exp(m\,L) + \beta \exp(-m\,L)\,. \end{aligned} \tag{24}$$

Combining equations (12) and (13), and taking the Laplace transform yields

$$M_U + M_W + M_S + M_D = \frac{V_U\, C_{U0}}{(s+\lambda)}, \tag{25}$$

where $M = \mathcal{L}\{m\}$. The summation terms on the left-hand side of equation (25) are:

$$M_U = V_U\, \Psi_0 = (\alpha + \beta)\, V_U\ , \tag{26}$$

$$\begin{aligned} M_W &= \phi\ [(1 - S_r) + S_r\, K_i] \int_0^L A\, \Psi dx \\ &= A\, \phi\, h \left\{ \frac{\alpha}{m} [\exp(m\, L) - 1] + \frac{\beta}{m} [1 - \exp(-m\, L)] \right\}, \end{aligned} \tag{27}$$

$$\begin{aligned} M_S &= (1 - \phi)\, \rho\, K_d\, K_i \int_0^L A\, \Psi dx \\ &= A\, \phi\, w \left\{ \frac{\alpha}{m} [\exp(m\, L) - 1] + \frac{\beta}{m} [1 - \exp(-m\, L)] \right\}, \end{aligned} \tag{28}$$

and

$$M_D = V_D\, \Psi_L = V_D\ [\alpha \exp(m\, L) + \beta \exp(-m\, L)]\,. \tag{29}$$

The Laplace transform of equation (17) yields

$$\begin{aligned} -\frac{m}{s}\, D^*\, A\, \phi\, [\alpha \exp(m\, L) - \beta \exp(-m\, L)] \\ = V_D\, [\alpha \exp(m\, L) + \beta \exp(-m\, L)] \left(1 + \frac{\lambda}{s}\right), \end{aligned} \tag{30}$$

from which

$$\alpha = \beta\, \gamma \exp(-2m\, L)\,, \tag{31}$$

where

$$\gamma = \frac{D^*\, A\, \phi\, m - V_D\, (s + \lambda)}{D^*\, A\, \phi\, m + V_D\, (s + \lambda)}\,. \tag{32}$$

For non-radioactive species, $\lambda = 0$, and equation (32) is simplified accordingly.

Substituting (26) through (29) in (25), using (31), and collecting and rearranging terms yields

$$\beta = \frac{V_U\, C_{U0}}{(s + \lambda)\, (P_1 + P_2 + P_3)}\ , \tag{33}$$

where

$$P_1 = [1 + \gamma \exp(-2m\,L)]\; V_U, \qquad P_2 = \frac{\phi\,A\,R^*}{m}\,[1 - \gamma \exp(-2m\,L)]$$
$$P_3 = \left[V_D\,(1+\gamma) - \frac{\phi\,A\,R^*}{m}\,(1-\gamma)\right] \exp(-m\,L). \tag{34}$$

The Laplace space solutions are thus given by

$$\Psi(x,s) = \beta\,\{\gamma \exp\,[m(x-2L)] + \exp(-m\,x)\}\;\;,$$
$$\Psi_0(s) = \beta\,[\gamma \exp(-2m\,L) + 1]\;\;, \tag{35}$$
$$\Psi_L(s) = \beta\,(1+\gamma)\exp(-m\,L)\;\;.$$

The same solution is obtained if, instead of the mass balance equation (25), the flux conditions at the $x = 0$ boundary are used. In this case, β is given by a different expression (see Appendix A), and all other terms remain unchanged. Equation (35) returns identical solutions for β either from equation (33) or from equation (A4).

3.2. Through-Diffusion With Linear Kinetic Sorption

Taking the Laplace transform of equations (7) and (19) leads to

$$D_T\,\frac{\partial^2\Psi}{\partial x^2} + D_F\,\frac{\partial^2\Theta}{\partial x^2} = h\,(s+\lambda)\,\Psi + \frac{(1-\phi)}{\phi}\,\rho\,(s+\lambda)\,\Theta\,, \tag{36}$$

and

$$s\,\Theta + \lambda\,\Theta = k\,K_d\,K_i\,\Psi - k\,\Theta \quad \text{and} \quad \Theta = \frac{k\,K_d\,K_i}{s+k+\lambda}\,\Psi\,, \tag{37}$$

where $\Theta = \mathcal{L}\{F\}$. Substituting (37) into (36) and rearranging terms yields

$$\frac{\partial^2\Psi}{\partial x^2} - \frac{\overbrace{h+u}^{R^*}}{D^*}\,(s+\lambda)\,\Psi = 0\,, \tag{38}$$

i.e., where

$$u = \frac{k\,K_d\,K_i}{s+k+\lambda}\,\frac{(1-\phi)}{\phi}\,\rho \qquad \text{and} \qquad D^* = D_T + \tau_s\,u\,D_s \tag{39}$$

In this case, the notion of the effective retardation factor R^* is expanded to describe time-variable behavior, and no longer conforms to its conventional meaning, as defined in linear equilibrium sorption scenarios. The mass balance equations, the only exception being equations (28), in which M_S is now given by

$$M_S = A\,\phi\,u\left\{\frac{\alpha}{m}\left[\exp(m\,L) - 1\right] + \frac{\beta}{m}\left[1 - \exp(-m\,L)\right]\right\}. \tag{40}$$

When the appropriate R^* (equation (38)) and D^* (equation (39)) terms are used, all the equations developed in the linear equilibrium problem apply unchanged to the case of linear kinetic sorption. The solution of Θ is then obtained from equations (35) and (37).

3.3. Through-Diffusion With Irreversible Sorption

In this case [*Bear*, 1979], the Laplace transform of the governing sorption equation (20) results in

$$\Theta = \frac{K_L\,K_i}{s+\lambda}\;\Psi, \tag{41}$$

where K_L is a constant $[L^3M^{-1}T^{-1}]$. Equation (44) indicates a solid phase acting as a sink for the dissolved species. Using an approach entirely analogous to that for diffusion with linear kinetic sorption, the solution is described by equation (35) when

$$R^* = h + v, \quad v = \frac{K_L\,K_i}{s+\lambda}\,\frac{(1-\phi)}{\phi}\,\rho \quad \text{and} \quad D^* = D_T + \tau_s\,v\,D_s\,. \tag{42}$$

In this case, M_S is given by equation (28) or equation (40), after substituting v for w or u, respectively. All other terms, parameters and equations defined in Section 3.2 apply unchanged. The solution of Θ is obtained from equations (35) and (41).

3.4. Extension to Reservoir Depletion and In-Diffusion Studies

Under these conditions (Figure 1b), the Laplace transform of equation (14) yields

$$-\frac{m}{s}\,D^*\,A\,\phi\,[\alpha\exp(m\,L) - \beta\exp(-m\,L)] = 0, \tag{43}$$

from which

$$\alpha = \beta \exp(-2m\,L)\,. \tag{44}$$

This is identical to (31) for $\gamma = 1$, which is obtained automatically when $V_D = 0$. The implication of this realization is that the solutions for Ψ in equation (35) and for Θ in equations (37) and (44), as well as all the associated terms corresponding to diffusion with (a) linear equilibrium sorption, (b) linear kinetic sorption, and (c) irreversible sorption, apply unchanged to reservoir-depletion and in-diffusion studies by setting $V_D = 0$.

3.5. Assumptions, Options and Simplifications

The solutions developed in this section are general, and applicable to diffusion in any closed system composed of upstream and downstream reservoirs (or a single upstream reservoir) of constant volumes and a PM sample of a finite length. A minimum of assumptions were involved in the development of the solutions, i.e.,

(1) the mass transfer between the mobile and immobile water fractions in the pores is described by the linear equilibrium of equation (6), and

(2) the concentration measurements do not necessitate solution sample removal (e.g., ion-specific electrodes [*McKinley and Swaminathan*, 1996]), or the sample volumes withdrawn for analysis are negligible compared to the reservoir volumes.

Simplification of the solutions is accomplished by an appropriate choice of values for the various parameters, without the need to alter the equations. Setting $\lambda = 0$ automatically provides the solutions to diffusion of non-radioactive solutes. When $K_i = 1$ and $S_r = 0$, no separate immobile water fraction is considered, and diffusion is assumed to occur uniformly in the pores of the PM. For $D_s = 0$, surface diffusion [*Jahnke and Radke*, 1987] is neglected. As has already been discussed, setting $V_D = 0$ provides the solution to the problem of diffusion in reservoir depletion and in-diffusion experiments (Figure 1b) without any

equation adjustments.

Note that although the focus is on diffusion experiments, the solutions are general and can accommodate any values for V_U, V_D, A and L. Thus, these equations can be used to investigate the performance of barriers in nuclear waste isolation applications.

Analysis of conventional diffusion results [*Skagius and Neretnieks*, 1986*a*; *McKinley and Swaminathan*,1996] involves information from the downstream reservoir (called the *measurement* reservoir) and allows the determination of composite terms rather than their respective components. For example, in the case of linear equilibrium, it is possible to determine R^* and D^* rather than the individual terms τ_p, τ_i, τ_s, D_s, K_d, K_i, and S_r (it is assumed that ϕ and D_0 are already available).

Unlike conventional techniques, the solutions discussed here allow the use of information from both the upstream and downstream reservoirs. Thus, it appears that it is possible to determine a larger number of direct (rather than composite) parameters by jointly inverting the upstream and downstream curves in an appropriate optimization scheme for parameter estimation. Certain simplifications may, however, be necessary to quantify some of the parameters if no independent evaluation is available. A common assumption is that the tortuosity factors $\tau_p = \tau_i = \tau_s = \tau$ [*Jahnke and Radke*, 1987], which could be determined from a ^3H or a I^- (non-sorbing) diffusion experiment. D_s is usually substantially smaller than D_0, and becomes important only when sorption is very strong [*Cook*, 1989].

4. Numerical Inversion of the Laplace Solutions

The time-variable concentrations can be determined by inverting the Laplace space solutions, i.e.,

$$\begin{aligned} C_U(t) &= \mathcal{L}^{-1}\{\Psi_0(s)\}, \qquad & C_D(t) &= \mathcal{L}^{-1}\{\Psi_L(s)\} \\ C(x,t) &= \mathcal{L}^{-1}\{\Psi(x,s)\}, \qquad & F(x,t) &= \mathcal{L}^{-1}\{\Theta(x,s)\}\,, \end{aligned} \tag{45}$$

where $\mathcal{L}^{-1}\{\}$ denotes the inverse Laplace transform of the quantity in the brackets. In diffusion cell studies, of particular interest are the $C_U(t)$ and the $C_D(t)$ solutions, from which the key diffusion and sorption parameters are deduced.

The complexity of the Laplace space solution precludes analytical inversion and the development of a closed-form equation. The problem is alleviated by numerically inverting the Laplace space solutions using one of the methods discussed below.

4.1. The Stehfest Algorithm

For a desired observation time t, the s in the Stehfest algorithm [*Stehfest*, 1970*a*; 1970*b*] is real and given by

$$s_\nu = \frac{\ln 2}{t} \cdot \nu, \qquad \nu = 1, \ldots, N_S \tag{46}$$

where N_S is the number of summation terms in the algorithm and is an even number.

When using the Stehfest algorithm, the inversion $Z(t)$ ($\equiv C, C_U, C_D, F$) of a Laplace space solution Υ ($\equiv \Psi$, Ψ_0, Ψ_L, Θ, respectively) at a time t is obtained from

$$Z(t) = \frac{\ln 2}{t} \sum_{\nu=1}^{N_S} W_\nu \, \Upsilon(s_\nu) \ , \tag{47}$$

where

$$W_\nu = (-1)^{\frac{N_S}{2}+\nu} \sum_{k=\frac{1}{2}(\nu+1)}^{\min\{\nu, \frac{N_S}{2}\}} \frac{k^{\frac{N_S}{2}}(2k!)}{(\frac{N_S}{2}-k)!k!(k-1)!(\nu-k)!(2k-\nu)!} \ . \tag{48}$$

Although the accuracy of the method is theoretically expected to improve with increasing N_S, *Stehfest* [1970*a*;1970*b*] showed that with increasing N_S the number of correct significant figures inreases linearly at first and then, due to roundoff errors, decreases linearly. He determined that the optimum N_S was 10 for single-precision variables (8 significant figures) and 18 for double-precision variables (16 significant figures). *Moridis*

and Reddell [1991] reported that the method seems to be insensitive to N_S for $6 \leq N_S \leq 20$ in the Laplace Transform Finite Difference (LTFD) method.

4.2. The De Hoog Method

In the method of *De Hoog et al.* [1982], hereafter referred to as the De Hoog method, s is a complex number given by *Crump* [1976] as

$$s_\nu = s_0 + \frac{\nu\pi}{T} j, \qquad s_0 = \mu - \frac{\ln(E_R)}{2T}, \qquad \nu = 1, \ldots, N_H \tag{49}$$

where $2T$ is the period of the Fourier series approximating the inverse function in the interval $[0, 2T]$, $j = \sqrt{-1}$, and $N_H = 2M_H + 1$ is an odd number. *Moridis* [1992*a*] showed that very accurate solutions were obtained when $\mu = 0$, $10^{-10} \leq E_R \leq 10^{-8}$, and $0.9\, t_{max} \leq T \leq 1.1\, t_{max}$, where t_{max} is the maximum simulation time.

The inversion of the Laplace space solution obtained with the De Hoog method is far more complicated than in the Stehfest algorithm. The solution $Z(t)$ is given by

$$Z(t) = \frac{1}{T} \exp(s_0 t)\, \mathrm{Re}\left[\frac{A_{2M}}{B_{2M}}\right], \tag{50}$$

where

$$A_n = A_{n-1} + d_n\, z\, A_{n-2}, \quad B_n = B_{n-1} + d_n\, z\, B_{n-2}, \quad n = 1, \ldots, 2M, \tag{51}$$

$$z = \exp\left(\frac{j\,\pi\,t}{T}\right) \tag{52}$$

$$A_{-1} = 0, \quad A_0 = d_0, \quad B_{-1} = B_0 = 1\,, \tag{53}$$

$$d_0 = a_0, \quad d_{2m-1} = -q_m^{(0)}, \quad d_{2m} = -e_m^{(0)}, \qquad m = 1, \ldots, M, \tag{54}$$

$$\begin{aligned} &\ell = 1, \ldots, M, \quad e_\ell^{(k)} = q_\ell^{(k+1)} - q_\ell^{(k)} + e_{\ell-1}^{(k+1)}, \quad k = 0, \ldots, 2M - 2\ell \\ &\text{for } \ell = 2, \ldots, M, \quad q_\ell^{(k)} = q_{\ell-1}^{(k+1)}\, e_{\ell-1}^{(k+1)} / e_{\ell-1}^{(k)}, \quad k = 0, \ldots, 2M - 2\ell - 1, \end{aligned} \tag{55}$$

$$e_0^{(k)} = 0 \text{ for } k = 0, \ldots, 2M \quad \text{and} \quad q_1^{(k)} = a_{k+1}/a_k \text{ for } k = 0, \ldots, 2M-1, \tag{56}$$

and

$$a_0 = \frac{1}{2}\Upsilon(s_0), \qquad a_k = \Upsilon(s_k). \tag{57}$$

A convergence acceleration is obtained if, on the last evaluation of the recurrence relations, $d_{2M}\ z$ in (51) is repaced by $R_{2M}(z)$,

$$R_{2M}(z) = -h_{2M}\left[1 - \sqrt{(1 + d_{2M}\ z/h_{2M})}\right], \tag{58}$$

where

$$h_{2M} = \frac{1}{2}[1 + z\ (d_{2M-1} - d_{2M})], \tag{59}$$

giving

$$\widehat{A}_{2M} = A_{2M-1} + R_{2M}\ A_{2M-2}, \qquad \widehat{B}_{2M} = B_{2M-1} + R_{2M}\ B_{2M-2}, \tag{60}$$

in which case the accelerated solution at a time t is given by replacing A_{2M} and B_{2M} by $\widehat{A}_{2M}$ and $\widehat{B}_{2M}$, respectively, in (50).

All the operations in equations (50) through (60) involve complex variables. *Moridis* [1992*a*] determined that the minimum M_H for an acceptable accuracy is 5 ($N_H = 11$), and that for an accuracy comparable to that of the Stehfest method $M_H \geq 6$ ($N_H \geq 13$). The unique advantages of the De Hoog formulation is that (a) it is capable of accurately inverting very steep solution surfaces, and (b) a whole range of solutions at times t in the range $[0, T]$ can be obtained from a single set of solutions Υ, i.e., equation (50) needs not be solved for each t of interest.

5. Verification and Analysis

A set of FORTRAN programs was written to obtain the semianalytical solutions by numerically inverting equation (35). These programs, as well as representative data files,

are available on the web at URL http://ccs.lbl.gov/Diffusion/. The standard parameter values used in the ensuing analysis appear in Table 1. Both the individual and the composite parameters (i.e., D^* and R^*) are shown. In the following sections, only parameters different from the standard ones are mentioned. To vary D^*, the value of D_0 is adjusted, but the tortuosity factors remain unchanged (see equations (8) and (18)). To vary R^*, only the K_d value is adjusted in equation (17).

5.1. Asymptotic Verifications

5.1.1. Through-Diffusion. The closed-form analytical solution of *Skagius and Neretnieks* [1986*a*] is based on the *Crank* [1975] solution, and is given by the equation

$$C_{RD} = \frac{C_D}{C_{U0}} = \frac{A\,L}{V_D}\left[\frac{\phi D^*\,t}{L^2} - \frac{\phi R^*}{6} - \frac{2\phi R^*}{\pi^2}\sum_{n=1}^{\infty}\frac{(-1)^n}{n^2}\exp\left(-\frac{D^*\,n^2\,\pi^2\,t}{L^2\,R^*}\right)\right], \tag{61}$$

which is valid when the conditions discussed in the introduction are met. For large t, the exponential components in (61) become negligible and D^* and R^* are determined from the slope and intercept, respectively, of the linear relationship of the C_{RD} vs. t curve.

Figure 2 shows a comparison of C_{RD} solutions obtained using equation (61) and of the solutions obtained by the inversion of equation (35) under through-diffusion conditions (hereafter referred to as the SA1 solution). The SA1 solutions of

$$C_{RU} = \frac{C_U}{C_{U0}}$$

are also shown.

Two general cases were investigated. In case 1, C_{RD} was determined from (61) for a through-diffusion system with the standard parameters (Table 1). To duplicate the conditions applying to (61), in the SA1 solution $V_D = 20\,m^3$ (case 1(a)). The two solutions are virtually identical, confirming the validity of the SA1 solution under these conditions.

The C_{RU} curve indicates practically constant upstream concentration during the duration of the diffusion, thus fulfilling the validity conditions of (61).

When the diffusion cell reservoirs have more realistic volumes in case 1(b), i.e., $V_U = V_D = 2 \times 10^{-3}\ m^3$, a small divergence of the two C_{RD} solutions is observed. Given the potential measurement errors, it appears that the divergence of the solutions is insufficient to substantially affect the accuracy of parameter prediction when using (61). What is more important, however, is the realization that the current practice of parameter estimation using equation (61) is unable to exploit the information from the variation in the value of C_{RU} from the upstream reservoir. This reduces the potentially available dataset by half, and produces inherently less accurate parameter estimates. Note that the underlying assumption of a constant $C_U = C_{U0}$ for a valid equation (61) is compromised.

In case 2, equation (61) is used to predict C_{RD} when $D^* = 5 \times 10^{-10}\ m^2 s^{-1}$ and all the other parameters remain unchanged. The SA1 solutions of C_{RD} and C_{RU} in case 2(a) use $V_U = V_D = 2 \times 10^{-3}\ m^3$, and show the substantial errors which (61) can introduce in the course of a through-diffusion cell experiment. While the slope of the two solutions about the origin are the same, the difficulty of obtaining accurate parameter estimates from (61) is obvious because (a) the representative portion of the curve is short (only 4 days in this case) and its duration is not known *a-priori*, (b) the first measurements are limited and have inherently larger measurement errors and scattering as downstream concentrations increase from 0, (c) an attempt to reduce data scattering and measurement errors by increasing the duration of the initial measurement period inevitably affects the quality of the parameter predictions as more non-linear data are interpreted using a linear model, and (d) information from the upstream reservoir (usually more reliable, as it involves a decrease from a larger and easier measured concentration) is not considered. Of particular interest is the fact that the magnitude of the C_{RU} signal can be linearly amplified by varying the absolute and relative sizes of V_D.

5.1.2. Reservoir Depletion and In-Diffusion. For an infinite-acting PM sample ($L \rightarrow \infty$), the depletion of a non-radioactive species (Figure 1b) is described by [*Lever*, 1986]

$$C_{RU} = \frac{C_U}{C_{U0}} = \exp\left(\frac{A^2\,\phi^2\,D^*\,R^*\,t}{V_U^2}\right)\,\mathrm{erfc}\left[\left(\frac{A^2\,\phi^2\,D^*\,R^*\,t}{V_U^2}\right)^{1/2}\right]. \tag{62}$$

By setting $\lambda = 0$, $V_D = 0$ and $\exp(-m\,L) = 1$, and using the Laplace transform property

$$\mathcal{L}\{s^{-1/2}\,(s^{1/2} + B^{1/2})^{-1}\} = \exp(B)\,\mathrm{erfc}(\sqrt{B}), \tag{63}$$

it is easy to show that Ψ_0 in equation (35) can be put in the form of the argument of $\mathcal{L}\{\}$ in equation (63), and thus (62) can be obtained from (35).

For confirmation, Figure 3 shows a comparison of the C_{RU} evolution over time computed from equation (62) and from SA1, i.e., the inversion of (35), for $L = 100\ m$. In addition to the SA1 solution, equation (35) was solved with $V_D = 0$ (hereafter referred to as the SA2 solution) and $L = 100\ m$ (i.e., practically infinite-acting). The remaining parameters in the SA2 solution and in equation (62) were as in Table 1. As expected, the three solutions coincide.

Figure 3 also shows the SA2 solutions for $L = 0.05\ m$ and $L = 0.02\ m$, while all the other parameters remain unchanged. It can be seen that when L is finite, equation (62) is initially accurate, but becomes increasingly inaccurate once the dissolved species front reaches the $x = L$ boundary.

5.2. Analysis of Through-Diffusion With Linear Equilibrium Sorption

5.2.1. Effect of D^*. Figure 4 shows the effect of D^* on the C_{RU} and C_{RD} solutions. As expected, higher D^* values correspond to faster changes in the concentrations of the reservoirs. For no sorption ($R^* = 1$), at equilibrium $C_{RU} = C_{RD} = V_U/(V_U + V_D)$.

In the case of Figure 4, due to sorption ($R^* = 3$), the final equilibrium concentrations $C_{RU} = C_{RD} < V_U/(V_U + V_D)$ due to the finite mass of the dissolved species.

5.2.2. Effect of Sorption. With increasing sorption (i.e., increasing R^*), both the C_{RU} and C_{RD} solution curves shift downwards (Figure 5), and the equilibrium concentration is thus reduced. This indicates faster concentration changes in the upstream reservoir and breakthrough delays in the downstream reservoir. The advantage of the SA1 solution of equation (35) over the traditional parameter estimation approach [*Skagius and Neretnieks*, 1986*a*] is obvious in the case of stronger sorption ($R^* = 100$). If used alone, the rapidly declining C_{RU} can provide faster and more accurate parameter estimates than the delayed C_{RD} breakthrough curve; when the two data sets are used together, more reliable estimates are possible.

It must be pointed out that Figure 5 (and even more so Figure 7, see next section) shows that the SA1 solution of C_{RU} is free of the most serious disadvantage [*Kirchner et al.*, 1996] of the conventional method of equation (61): that the time needed to establish steady-state may be excessively (and impractically) long for strong adsorbers [*Put and Henrion*, 1988]. On the contrary, stronger sorption accelerates the rate of C_{RU} change in SA1, thus reducing accordingly the data aquisition time.

5.2.3. Effect of Surface Diffusion. The significance of surface diffusion in the performance of barriers in nuclear waster isolation applications was recognized rather recently [*Lever*, 1986; *Jahnke*, 1986; *Jensen and Radke*, 1988; *Jahnke and Radke*, 1987; *Berry and Bond*, 1992]. When sorption is very strong (i.e., large R^* values), it can be shown that the apparent diffusion coefficient $D_A = D^*/R^* \rightarrow \tau_s D_s$ in equation (16), i.e., surface diffusion is responsible for practically all the diffusion despite the fact that D_s is usually substantially smaller than D_0. The implication of this realization is that the diffusion of a strongly sorbed species through a PM which supports surface diffusion may be much faster than would be predicted on the basis of batch sorption experiments and reasonable

D_0 values [*Cook*, 1989].

Figure 6 shows the effect of surface diffusion on the C_{RU} and C_{RD} solutions for $R^* = 10$ and 100, corresponding to $K_d = 1.8639 \times 10^{-3}\ m^3 kg^{-1}$ and $2.0503 \times 10^{-2}\ m^3 kg^{-1}$, respectively. D_T is maintained constant at $10^{-10}\ m^2 s^{-1}$, and $D_s = 0.1\, D_0$. The C_{RU} and C_{RD} curves with and without surface diffusion tend to the same equilibrium values. Although D_s is small compared to D_0, its effect on the acceleration of equilibrium in the concentration of both reservoirs is substantial and easily measurable. It can be seen that the accelerating effects are amplified when sorption becomes stronger. For $R^* = 100$, the evolution of C_{RD} over time indicates a substantially faster breakthrough (by about an order of magnitude). Of particular interest is the C_{RU} curve, which is characterized by a steep initial decline, followed by a more gradual decrease. Although the equilibrium concentrations with and without surface diffusion are the same, the decline in the C_{RU} curve with $D_s = 0.1\, D_0$ is substantially faster. The advantage of using both C_{RU} and C_{RD} for parameter estimation is obvious, as the surface diffusion process can be captured and described by the combination of the two curves, and especially by the faster, large and easy-to-measure changes in C_{RU}. Using only the information from the C_{RD} curve may not suffice to differentiate the pore and surface diffusion processes [*Lever*, 1986].

When $C_U(t) = C_{U0}$ and sorption is very strong, the transport rate is controlled only by $D_A \simeq \tau_s\, D_s$ and does not decrease as sorption increases. This attribute has been used to identify and measure surface diffusion [*Muurinen et al.*, 1989]. In diffusion cells with a finite dissolved species mass this is not the case because a significant portion of its mass is removed from solution as it sorbs onto the PM.

The behavior of the C_{RU} and C_{RD} solutions under conditions of very strong sorption and surface diffusion is shown in Figure 7. In Figure 7, the 'u' and 'd' denote C_{RU} and C_{RD} curves respectively; '1', '2' and '3' indicate a $K_d = 5.1568 \times 10^{-2}\ m^3 kg^{-1}$ ($R^* = 250$), 1 $m^3 kg^{-1}$ (e.g., Pu sorption onto Yucca Mountain vitric tuffs [*Triay et al.*, 1996], $R^* = 4829$),

and 3 m^3kg^{-1} (e.g., Cs sorption onto a Na bentonite [*Torstenfelt*, 1986], $R^* = 14486$), respectively; 'S' indicates the presence of surface diffusion, with $D_s = 0.1\,D_0$; and 'C' denotes the conventional solution of equation (61).

Under the conditions of equation (61), the curves for $R^* = 250$, 4829 and 14486 in Figure 7 are d1S-C, d2S-C and d3S-C, respectively, and the downstream cell is the only source of information. These curves are obtained from the SA1 solutions by setting $V_U = 200\ m^3$, i.e., $C_U \simeq C_{U0}$. While it is possible to differentiate d1S-C, the d2S-C and d3S-C curves coincide, in agreement with previous observations [*Muurinen et al.*, 1989]. The conventional approach is incapable of differentiating between different PMs once sorption becomes sufficiently high ($R^* \geq 800$) in PMs which support surface diffusion (e.g., bentonite-based barriers). Additionally, it is hampered by long breakthrough times, as well as the difficulties of obtaining accurate data from at low concentrations.

When a closed diffusion cell system is used and C_{RU} is measured, it is easy to differentiate between PMs even under conditions of surface diffusion and extremely high sorption, an impossible task for the conventional approach. In Figure 7, the C_{RU} curves for $R^* = 250$, 4829 and 14486 with surface diffusion (i.e., curves u1S, u2S and u3S, respectively) show significant separation from each other, in addition to being distinctively different from the corresponding curves for the same R^* but with no surface diffusion (curves u1, u2 and u3, respectively). The presence of surface diffusion significantly decreases C_{RU} under strong sorptive conditions. A distinctive feature of these two sets of curves is that the stronger the sorption is, the faster and more pronounced is the effect on C_{RU}, i.e., the opposite of what occurs in conventional analysis of C_{RD}.

Compared to the conventional breakthrough curves (i.e., d1S-C, d2S-C and d3S-C), the behavior of C_{RD} in closed systems shows a substantial delay. This delay increases with sorption. When surface diffusion is not considered, only the C_{RD} curve for $R^* = 250$ (curve d1) shows a clear and measurable breakthrough, while no breakthrough occurs for

$R^* = 4829$ and $R^* = 14486$ within the time-frame of the observation. The presence of surface diffusion accelerates the emergence of a breakthrough (curve d1S), which occurs roughly at the same time as for the d1S-C curve but exhibits a much slower rate of increase. This is due to the significantly smaller equilibrium concentration in the downstream reservoir because of the fixed mass and the strong sorption of the dissolved species. Note that the C_{RD} curves for $R^* = 4829$ and $R^* = 14486$ with surface diffusion are shown in the lower right corner of Figure 7 but can be barely differentiated from the $x = 0$ axis.

The practical implication of these realizations is that a closed system with a fixed species mass allows the differentiation and parameter estimation of systems with strong sorption and surface diffusion. C_{RU} measurements allow fast and accurate parameter estimation. As stronger sorption increases the rate of C_{RU} change (e.g., in u3S, $C_{RU} = 0.162$ at $t = 0.02$ days), equation (35) can be used to determine the absolute and relative reservoir sizes (i.e., V_U and V_D) for optimum data quality within a desired sampling period. Although the C_{RD} data can provide a useful second data set for more reliable parameter estimates, the long time for data aquisition and the larger measurement errors at low concentrations limit their usefulness.

It is also important to note that these results indicate that the traditional approach of evaluating the performance of a diffusion barrier material in terms of K_d may not be relevant in the presence of surface diffusion. A larger K_d clearly indicates stronger sorption, but this does not mean immobilization of the dissolved species when the PM supports surface diffusion. On the contrary, the stronger the sorption (i.e., the larger the K_d), the larger the diffusion rate will be, and practically all of it due to the surface process. This counterintuitive observation confirms previous work on the subject [*Jahnke and Radke*, 1987; *Cook*, 1989].

5.2.4. Effect of Immobile Water Fraction. It is obvious that the presence of an immobile water fraction would result in lower diffusion (equation (8)) and lower sorption (equation (18)) due to the limited mass transfer of dissolved species between the mobile

and immobile water pore fractions. This is demonstrated in Figure 8, which the effect of K_i and S_r on the C_{RU} and C_{RD} solutions for two different K_d values.

For a low-sorbing system ($K_d = 1.86 \times 10^{-3}\ m^3\ kg^{-1}$), a $K_i = 0.1$ and $S_r = 0.2$ ($R^* = 1.718$, $D_T = 0.082\ D_0$) shifts the C_{RU} curve measurably upward compared to the case of $K_i = 1$ and $S_r = 0$ ($R^* = 10$, $D_T = 0.1\ D_0$, i.e., when no immobile fraction is considered). This indicates a lower rate of species depletion, and is in accordance with expectations based on the lower R^* and D_T values. The C_{RD} solutions, though, are practically indistinguishable, and it is doubtful whether measurement methods are sufficiently accurate to differentiate the two.

The effect of the immobile water fraction is far more pronounced in the case of stronger sorption ($K_d = 2.05 \times 10^{-2}\ m^3\ kg^{-1}$). A change from $K_i = 1$ and $S_r = 0$ ($R^* = 100$, $D_T = 0.1\ D_0$) to $K_i = 0.1$ and $S_r = 0.2$ ($R^* = 10.72$, $D_T = 0.082\ D_0$) in essence reduces sorption by a factor of about 10, and results in the significant difference between the two sets of C_{RU} and C_{RD} solutions. The effect of the reduced D_T is substantially smaller.

A point which must be made clearly is that the immobile fraction affects the composite terms R^* and D^*, which are the only ones that can be determined from the analysis of the diffusion cell results. For a known D_0 and $\tau_p = \tau_i$ (from a diffusion experiment of the same PM with a non-sorbing species), the K_i and S_r can be evaluated using both the C_{RU} and C_{RD} curves for maximum accuracy and reliability.

5.2.5. Effect of Radioactive Decay. Figure 9 shows the effect of radioactive decay on the C_{RU} and C_{RD} solutions for (a) a non-sorbing ($R^* = 1$) species with $T_{1/2} = 12.32$ yrs (^{3}H) and (b) a strongly sorbing ($R^* = 250$) species with $T_{1/2} = 2.065$ yrs (^{134}Cs). The C_{RU} and C_{RD} curves for the non-radioactive species with the same sorption behavior are also included for reference.

Within the duration of most diffusion experiments (≤ 1 yr), the C_{RU} curves of the radioactive and the non-radioactive non-sorbing species exhibit no measurable differences.

The same is observed for the C_{RD} solutions. The differences begin to be measurable at impractically long observation times ($t \geq 500$ days). On the other hand, measurable differences are observed within a year in the case of the strongly sorbing species with the shorter half-life, and especially in the in C_{RU} curves.

The practical implication of these observations in diffusion cell data analysis is that radioactive decay has to be accounted for if the half-life is significant compared to the experiment duration. Otherwise, the data may be misinterpreted as indicating stronger apparent diffusion and/or sorption.

5.2.6. Effect of Cell Design and Geometry. Because of the finite mass of dissolved species, the specifications of the diffusion cell can be altered in order to optimize the data quality and aquisition. We use as an example the case of surface diffusion ($D_s = 0.1D_0$) under conditions of very strong sorption, i.e., $R^* = 4829$ and $R^* = 14486$ (see Section 5.2.3). From Figure 7, we notice that the response of C_{RU} (curves u2S and u3S) may be too rapid for reliable and convenient data aquisition, and that it declines to very low (and inherently difficult to measure) levels within a few days, thus reducing the volume and possibly the quality of obtainable data.

Figure 10 shows the effect of adjusting the V_U and V_D volumes on the C_{RU} and C_{RD} curves. When V_U increases from 0.002 m^3 (2 L) to 0.004 m^3 (4 L) and V_D decreases from 0.002 m^3 to 0.001 m^3 (1 L), both the C_{RU} and the C_{RD} curves shift upwards, thus providing higher readings (easier and more accurate to measure) over a longer time. This agrees with expectations, as more species mass is now available in the upstream reservoir, while a stronger response is expected in the smaller downstream reservoir. Additionally, C_{RD} measurements can be made at an earlier time, thus reducing the duration of the experiment while providing information from both reservoirs. Increasing V_U to 0.006 (6 L) m^3 while maintaining $V_D = 0.001$ m^3 shifts the C_{RU} and C_{RD} curves even higher and allows better-controlled data aquisition under conditions of very rapid C_{RU} signal change.

The effect of the cross-sectional area of diffusion A appears in Figure 11 for the same conditions of sorption and diffusion discussed in Figure 10, and for $V_U = V_D = 0.002\ m^3$. By reducing A from 0.01 m^2 to 0.008 and 0.005 m^2, the PM mass is reduced, and the dissolved species mass sorbed on the PM sample is accordingly reduced. This results in the significant upward shift of the C_{RU} curves shown in Figure 11. The effect on the C_{RD} curves is far less pronounced, and evident only at later times, i.e., reducing A does not appear to advance the onset of data aquisition.

The practical implications of the analysis of Figures 10 and 11 is that manipulation of the geometric features of the diffusion cell allows control over the duration of the experiment and the data quality. Note that it is not necessary for V_U and V_D to be fixed cell specifications. It is easy to increase V_U and V_D by connecting the fixed reservoirs in Figure 1(a) with external reservoirs and maintaining liquid circulation. In this case, V_U and V_D in equation (35) are taken as the sums of the fixed and external reservoir volumes.

5.3. Analysis of Through-Diffusion With Linear Kinetic Sorption

In the conventional analysis of the vast majority of diffusion experiments, it is assumed that the sorption processes are instantaneous, reversible, and represented by a linear isotherm [*Shackelford*, 1991; *Kirchner et al.*, 1993]. The importance of non-linear and kinetic sorption processes in diffusion experiments, especially in cases of strong adsorption in nuclear waste applications, has only recently been realized [*Kirchner et al.*, 1996], and the existing body of literature is limited [*Smith*; 1990; *Kirchner et al.*, 1996].

In this section, we discuss through-diffusion experiments with linear kinetic sorption using the semi-analytical SA1 solution involving the numerical inversion of the Laplace space equation (35) and the terms defined in Sections 3.1 and 3.2. An analysis similar to that for linear equilibrium sorption can be conducted. The following discussion is limited

to an analysis of issues important to nuclear waste applications, and their implication for the interpretation of the results of diffusion experiments.

5.3.1. Effects of Kinetic Constant k for Varying Distribution Coefficients K_d. Figures 12, 13 and 14 show the effects of a varying k in systems with $K_d = 1.8639 \times 10^{-3}$, 5.1568×10^{-2} and $1\ m^3 kg^{-1}$, respectively. When at equilibrium, these K_d's correspond to an R^* of 10, 250 and 4829, respectively. The effect of varying k is investigated by obtaining the SA1 solutions of C_{RU} and C_{RD} from equation (35) for $k = k_1$, k_2, k_3 ($k_1 = 10^{-5}$ s^{-1}, $k_2 = 10^{-8}\ s^{-1}$, $k_3 = 10^{-10}\ s^{-1}$). For comparison, the solutions when $V_U = 200$ m^3 (i.e., when the upstream concentration is kept constant) are also included in the figures, and are denoted by an asterisk for the corresponding k (e.g., k_{1*} denotes the solution when $k = k_1$ and $C_U = C_{U0}$). The latter represent the anticipated experimental observations in conventional diffusion experiments.

Figure 12 indicates that lower k values cause the C_{RU} and C_{RD} curves to shift upward, in accordance with expectations. It is important to note that the effects of varying k by several orders of magnitude are not significant when sorption is not strong. The differences between the curves appear to become measurable for $t > 200$ days, i.e., near the upper limit of duration for most diffusion experiments. Given the usual levels of experimental accuracy, it is unlikely that the C_{RU} and C_{RD} curves can provide sufficient information to determine the kinetic character of the sorption process (as the solution curves are quite similar to those for equilibrium sorption) and to accurately determine k and K_d. If the fact that sorption is kinetically controlled cannot be independently established, it is quite possible to misinterpret the measurement data by using a linear equilibrium model.

Figure 12 also shows that it is extremely difficult to infer the kinetic character of sorption (let alone the k values) from the C_{RD} measurements when $C_U = C_{U0}$, as the curves are very close to each other, have no distinguishing characteristic, and can be easily misinterpreted by inappropriately using the linear equilibrium model of equation (61). The

problem persists in the stronger sorption environment of Figures 13 and 14, where the curves for $C_U = C_{U0}$ indicate a slow breakthrough and demonstrate inability to either describe the kinetic character of sorption or quantify it.

The SA1 solutions for C_{RU} and C_{RD} in Figures 13 and 14 demonstrate a fast response. The curves are measurably different with varying k, and this curve differentiation increases with K_d (Figure 14). For smaller k values, C_{RD} (and occasionaly C_{RU}) demonstrates a distinctive *hump* shape, caused by diffusion from the downstream reservoir back toward the PM sample as sorption increases with time until equilibrium. This may allow the identification of sorption as kinetically controlled, as well as the determination of k and K_d by jointly inverting both the C_{RU} and C_{RD} curves. Unfortunately, this occurs at times well outside the practical time-frame of most diffusion experiments.

The duration of most diffusion experiments is such that the C_{RU} and C_{RD} measurements could be interpreted by using either an equilibrium or a kinetic model, as the data set is insufficiently long to capture the particularities of kinetic behavior. The choice of the model may be of critical importance in diffusion studies for nuclear waster isolation. The inability to unequivocally identify the sorption process within a practical time-frame necessitates an independent determination of its equilibrium or kinetic behavior. Evidence of kinetic behavior can be provided by conducting batch sorption experiments and analyzing the results using a linear equilibrium model. A time-variable K_d, increasing with time (and then possibly stabilizing) is a necessary (though not sufficient) indication of kinetically controlled sorption. Once this is established, joint inversion of the C_{RU} and C_{RD} measurements allows the determination of k and K_d.

Figure 15 shows the ratio $M_{RSW} = m_S/m_W$ of the adsorbed species mass to its dissolved mass in the pore waters of the PM sample for the examples discussed in Figures 12 through 14. As expected from the underlying linear kinetic model, M_{RSW} first increases and then reaches a maximum constant level. Stronger sorption (i.e., a larger K_d) increases

M_{RSW} and raises the level of the plateau. A lower k shifts the rising portion of the M_{RSW} curves downward (i.e., lower values at the same t), and thus delays reaching the plateau.

5.3.2. Kinetically-Controlled Sorption and Surface Diffusion. The effect of surface diffusion in PM system with kinetically controlled sorption is demonstrated in Figures 16 and 17 for $K_d = 5.1568 \times 10^{-2}$ and 1 $m^3 kg^{-1}$, respectively. The C_{RU} and C_{RD} curves were obtained for $D_s = 0.1\, D_0$, $V_U = 0.02\ m^3$ (i.e., $V_U = 10V_D$), and for $k = k_1, k_2, k_3$ (defined in Section 5.3.1).

Of particular interest is the oscillatory behavior of C_{RD} (and, to a far lesser extent, of C_{RU}) for k_2 and k_3, i.e., for slower kinetic rates. This is akin to oscillatory chemical and geochemical systems, for which a substantial body of literature is available [*Fisher and Lasaga*, 1981;*Ortoleva*, 1994]. The oscillations are eventually attenuated, and the system reaches equilibrium. For $K_d = 5.1568 \times 10^{-2}\ m^3 kg^{-1}$ and $k = k_3$, the time to equilibrium is extremely long ($> 10^6$ days). When the kinetic rate is high ($k = k_1$), no such oscillations are observed.

A related significant item is the observation that in such systems C_{RD} can occasionally exceed 1, indicating downstream concentrations higher than C_{U0}. This is an intruiging observation. In Figure 18, an analysis of the species mass in the various components of the diffusion system (i.e., m_U, m_W, m_S, and m_D) for the PM with $K_d = 1\ m^3 kg^{-1}$ and $k = k_3$ (see Figure 17) indicates that they do not exhibit a non-physical behavior and that mass balance is maintained (i.e., m_T is constant) at all times ($C_{U0} = 1\ kg \cdot m^{-3}$).

Thermodynamic analysis of the system showed an increase in the total entropy, thus the third law of thermodynamics is not violated. When the same problem was solved numerically using a general-purpose simulator [*Pruess*, 1991] with an appropriate solute transport module [*Moridis et al.*, 1998], identical solutions were obtained. Study of Figures 17 and 18 indicate that the sorbed species mass m_S increases monotonically. At the peak $C_{RD} \simeq 1.2$, m_S is about 2 orders of magnitude larger than m_W, and m_D about an order of

magnitude smaller than C_{RU}. Note that at $t = 10^4$ days, the species mass in the upstream reservoir ($V_U = 2 \times 10^{-2}\, m^3$) is equal to the mass sorbed on the PM which is only $L = 10^{-2}$ m across.

The concentration ocsillations are evident in Figure 19, which shows the spatial and temporal variation of the concentration in the pore water of the PM sample with $K_d = 1$ $m^3 kg^{-1}$ and $k = k_3$. The relative concentration $C_{RP} = C(x)/C_{U0}$ initially follows the concentration gradient in the reservoirs. This is later reversed, and C_{RP} peaks at $x = L$ and at about $t = 1000$ days (Figure 19a). This cycling continues (Figure 19b), and eventually the oscillations are attenuated as the system reaches equilibrium.

Contrary to Figure 19, the concentration of the sorbed species in Figure 20 (expressed as $F_{RS} = F/C_{U0}$) shows practically imperceptible oscillations, very mild spatial variations across the length of the sample, and a monotonically increasing pattern over time (which continues to equilibrium). It appears that the concentration fluctuations are necessary to support the relatively stable F_{RS} imposed by the sorption kinetics and the surface diffusion. Note that at the C_{RP} and the F_{RS} curves have opposite slopes when C_{RP} oscillates, and that these oscillations do not appear to have an effect on the slope or magnitude of F_{RS}.

It appears that this oscillatory behavior is unique to PM systems which support surface diffusion and have kinetically controlled sorption. While this behavior is mathematically possible and was obtained using reasonable diffusion and sorption parameters, it is not known whether such systems occur naturally and caution should be exercized. To the author's knowledge, no such oscillatory behavior has been reported in the diffusion literature. That would have been unlikely, as the time frame for the appearance of these oscillations exceeds the duration of most diffusion experiments. Such behavior, if it can be experimentally confirmed, could have significant implications in the design and performance of barriers for nuclear waste isolation, as bentonite (a common barrier material) is known to support surface diffusion [*Jehnsen and Radke*, 1986].

5.4. Analysis of Through-Diffusion With Irreversible Sorption

In such a system, the solid phase acts as a sink for the dissolved species [*Bear*, 1979]. The SA1 equations with the adjustments discussed in Section 3.3. can be used to describe mathematically (but not necessarily physically or chemically) a combination of sorption and precipitation as a reactant moves through a PM, provided F can be described by equation (44) with appropriate parameters.

The analysis of such a system can be made in a manner entirely analogous to the one discussed in Sections 5.2 and 5.4. For the sake of completeness, we include Figure 21, which shows the response of C_{RU} and C_{RD} for $K_L = 10^{-5}$, 10^{-6}, 10^{-8} and 10^{-10} $m^3kg^{-1}s^{-1}$. It can be seen that C_{RU} declines to zero for all K_L values, and no C_{RD} breakthrough occurs for $K_L > 10^{-10}$ $m^3kg^{-1}s^{-1}$. This is due to the high values of the transfer rate constant K_L, which causes the rapid removal of the dissolved species from the solution. For $K_L = 10^{-10}$ $m^3kg^{-1}s^{-1}$, sorption is slow compared to diffusion, and a breakthrough is observed starting at about $t = 8$ days. As irreversible sorption continues, the dissolved species is sorbed onto the PM, and eventually both C_{RU} and C_{RD} tend to zero.

5.5. Analysis in Reservoir-Depletion and In-Diffusion Experiments

As was discussed earlier, the reservoir-depletion and in-diffusion (SA2) solutions are a subset of the through-diffusion (SA1) solutions, from which they are obtained by setting $V_D = 0$. It follows that an analysis of the SA2 solutions under (a) equilibrium, (b) linear kinetic, and (c) irreversible sorption can be conducted in a manner analogous to the ones described in Sections 5.2, 5.3, and 5.4. It is obvious that this type of diffusion study is applicable to cases of strong sorption. Otherwise, the very limited volume of the sample would have a limited (and potentially undetectable) effect on the upstream concentration.

Of interest is the application of the solution of equation (35) in scoping calculations to determine the effect of diffusion in the transport of radionuclides. The case investigated here is that of Retention Basin 281-3H (hereafter referred to as the H-basin), a shallow catchment basin at the Savannah River Site (SRS) of the U.S. Deprtment of Energy in South Carolina, the isolation of which provided the initial impetus for this study. The H-basin was originally built to control contaminated runoff from the H Reactor, and has been contaminated mainly by ^{137}Cs and ^{90}Sr. A detailed description of the pond, contamination, and the prevailing conditions at the site can be found in *Moridis et al.* [1996].

The pond dimensions are $60 \times 36 \times 2$ m, and the average water depth is $0.6\ m$. Rainfall in that area averages 1.15 m/year, and is assumed to replenish evaporation losses. Most of the contamination was believed to be confined within the first 0.3-0.6 m from the basin bottom and walls.

Assuming that the water level in the basin coincides with the groundwater level, and neglecting advection, equation (35) can be used to determine the minimum extent (best-case scenario) of radionuclide transport and distribution. The actual transport is expected to be higher because of advection. Based on the volume of water in the basin, the cross-sectional area corresponding to each m^3 of water in the basin is $1.75\ m^2$. The soil in the H-basin area is mainly kaolinitic clay, which has limited ion-exchange capacity [*Moridis et al.*, 1996]. Batch sorption experiments showed that ^{90}Sr sorption is linear, with $K_d = 10^{-3}\ m^3/kg$ [*Hakem et al.*, 1997].

In equation (35), $\phi = 0.38$, $\rho = 2600\ kgm^{-3}$, $D^* = 10^{-10}\ m^2s^{-1}$, $D_s = 0$, $S_r = 0$, $V_U = 1\ m^3$, $A = 1.75\ m^2$, and $L = 100\ m$ (i.e., practically infinite). V_D was set to zero (SA2 solution), although identical results are obtained for $V_D \neq 0$ because of the very large L. For ^{90}Sr, $T_{1/2} = 29.1$ years, corresponding to $\lambda = 7.5 \times 10^{-10}\ s^{-1}$.

Figure 22 shows that C_{RU} in the H-basin after 10^5 days (273.8 yrs) is about 5×10^{-4}, which could be substantial if C_{U0} (which is not yet fully determined) is high. The spatial

distribution of C_{RP} $(= C(x)/C_{U0})$ over time is shown in Figure 23, and indicates that at $t = 10^4$ days (roughly the time since the releases into the basin), the extent of contamination is limited to less than 1 m from the basin bottom and walls. Note that at $t = 10^5$ days, the contamination is limited to the top $3 - 3.5$ m from the contact area, but its levels could be substantial depending on the C_{U0}. Because of linear sorption, the amount of sorbed species is directly proportional to C_{RP}, and $m_S/m_P = 3.56$, i.e., the sorbed species mass is 3.56 times larger than the mass in the pore water. This can be easily seen in Figure 24, which shows the relative masses $m_{Ri} = m_i/m_0$, $i \equiv U, P, S, T$, where $m_0 = V_U\, C_{U0}$, i.e., m_T at $t = 0$.

5.6. Comparison of the Inversion Schemes

The solutions presented up to now were obtained by inverting equation (35) using the De Hoog method with $M_H = 20$ $(N_H = 41)$, $E_R = 10^{-9}$ and $T = t_{ob}$, where t_{ob} is the time of observation. This will be referred to as the standard solution. Although the De Hoog method allows computation of the solution over the whole range of $0 \leq t_{ob} \leq t_{max}$, the accuracy deteriorates if $t = t_{ob}$ in equation (53) and T are not of the same order of magnitude [*Moridis*, 1992*b*]. To minimize machine accuracy errors as t becomes large, the unit of time in the solutions was days instead of s. The value of $M_H = 20$ was chosen because, in earlier tests [*Moridis*, 1992*b*], it had been determined to successfully invert the Laplace transform of the step function (the most challenging inversion problem available) with an error of less than 10^{-4} %.

The standard solution was compared to the C_{RU} and m_T solutions obtained from the inversion of equation (35) using (a) the De Hoog method for $6 \leq M_H \leq 22$ and (b) the Stehfest algorithm for $6 \leq N_S \leq 22$. The problem used in these comparisons was of that through diffusion with linear equilibrium sorption ($R^* = 100$) and no surface diffusion (see

Section 5.2.2 and Table 1).

Figure 25 shows that for $M_H = 6$, the absolute deviation of C_{RU} from the standard solution was less than 4×10^{-5} %, and that for $M_H = 8$ a few individual solutions exhibited deviations as t grew larger, but did not exceed 3×10^{-7} %. For $M_H > 8$, the solutions were identical in at least the first 8 significant digits and are not included in Figure 25. The same pattern was observed in the study of the effect of M_H on the mass balance (i.e., m_T). Compared to the standard solution, m_T was invariable for $M_H > 6$ over the range of time, and showed an absolute deviation of less than 3×10^{-7} % for $M_H = 8$.

The Stehfest inversion of equation (35) exhibits a more complicated picture. From Figure 26(a), it can be seen that the C_{RU} solutions shows significant deviations from the standard solution for $N_S = 6$. These deviations decrease with an increasing N_S. For $N_S = 14$, the deviations are less than 10^{-6} for $t < 300$ days, but increase rapidly for longer times, although they exhibits a series of local minima. The same pattern is observed for $N_S = 16$ in Figure 26(b), which, however, demonstrates somewhat higher deviations that increase rapidly for $t > 800$ days. For $N_S = 18$, however, the absolute deviation fluctuates around 2×10^{-4} %, i.e., it is higher than those for $N_S = 14$ or $N_S = 16$, but is relatively stable over the time range studied here. It appears that the number of summation terms is insufficient to counteract roundoff error as t increases for $N_S \leq 16$. For $N_S > 18$, the deviations increase with N_S due to larger roundoff errors [*Stehfest*, 1970*a*].

Of interest is the effect of N_S on the deviations of m_T from the standard solution. Figure 27(a) includes only the curve for $N_S = 14$ because the deviations are less than 10^{-7} % for $6 \leq N_S < 14$. This clearly indicates that for these low N_S values, the Stehfest inversion of (35) produces solutions which are inaccurate, but still maintain mass balance. The consequence of this observation is that mass balance alone is an insufficient indicator of an accurate solution. For $N_S \geq 16$, the deviations of m_T from the standard solution, both in terms of pattern and magnitude, are remarkably similar to that of C_{RU}, and seems

to be unaffected by t.

The implication of these results for the choice of the inversion method is that, with an appropriate choice of parameters, both methods produce accurate solutions, which differ in the fourth decimal place and beyond, i.e., they are practically identical. The Stehfest solution has the additional advantage of simplicity and ease of coding, while execution speed is not a consideration because both inversions are very fast (requiring less than 2 s to invert equation (35) at 500 t_{ob} points). On the other hand, if very high accuracy (and especially at very low C_{RU} and C_{RD} levels) is required, the Stehfest solution may not be the appropriate choice, as it oscillates about zero when C_{RU}, $C_{RD} < 10^{-6}$. In this case, the De Hoog inversion is a better choice.

Regarding the parameters of the inversion schemes, a $N_S = 18$ appears to give the best overall performance in the Stehfest algorithm. This is the optimum value suggested by *Stehfest* [1970*a*] for double precision arithmetic. For the De Hoog method, $E_R = 10^{-9}$ and $T = 2\ t_{ob}$ appear to give excellent results, while a $M_H = 10$ or 12 appears to be adequate for most applications, and provides accurate, non-oscillatory C_{RU} and C_{RD} results at the 10^{-14} level. Increasing M_H does not lead to roundoff errors, but increases the accuracy of the solution.

6. Estimation of Diffusion and Sorption Parameters

The estimation of parameters from experimental data, i.e., the inverse problem, is demonstrated in this example. The extreme non-linearity of the solution and the number of parameters involved (although it is possible to reduce their number by estimating the composite parameters) preclude the use of a trial-and-error approach. The non-linear optimization technique of *Thomas and Hellums* [1972] was coupled with the semi-analytical solution, and by history-matching experimental data and the SA1 predictions (i.e., numerical

inversions of equation (36)), an appropriate objective function was minimized, and the diffusion and sorption parameters were estimated.

The experimental data from a through-diffusion experiment were obtained by *McKinley and Swaminathan* [1996] in their study of rock matrix diffusion of Pb and Cd through shales for the deep injection of wastes. The particular data set used for history matching corresponded to a shale from Du Pont's Beaumont works in Texas, taken from a depth of 3646 ft (1111 m). As this experiment used the conventional approach, a linear equilibrium model was assumed and only C_{RD} measurements were made. Using equation (61) (simplified by the omission of the exponential terms) and the corresponding empirical determination of the slope and intercept of the C_{RD} vs. t curve, *McKinley and Swaminathan* [1996] determined that for Pb

$$\phi D^* = 5.83 \times 10^{-10}\, m^2 s^{-1} \quad \text{and} \quad \phi R^* = 19.2 \quad .$$

From previous batch experiments, it had been determined that $\phi = 0.41$ and that sorption had a linear equilibrium isotherm with a $K_d^b = 5.2 \times 10^{-2}\, m^3 kg^{-1}$. Using this value of ϕ, the diffusion experiment yields

$$D^* = 1.42 \times 10^{-9}\, m^2 s^{-1} \quad \text{and} \quad R^* = 46.8,$$

from which $K_d^d = 1.225 \times 10^{-2}\, m^3 kg^{-1}$, i.e., the K_d from the diffusion experiment is 4.25 times smaller than that determined from the batch experiment. When these values were used in equation (35), the SA1 solution (designated in Figure 28 as the curve with D^*, K_d from M+S) showed significant deviation from the experimental data.

Three sets of history-matching runs were conducted. The non-varying parameters for the history-matching iterations are shown in Table 2. In the first set, linear equilibrium sorption was assumed, and K_d was kept fixed at the value determined from the batch experiments, i.e., $K_d = 5.2 \times 10^{-2}\, m^3 kg^{-1}$. The parameter allowed to vary was D_0 (=D^* for $\tau_p = 1$), which had as initial value that determined from the analysis of the diffusion

experiment of *McKinley and Swaminathan* [1986], i.e., $D^* = 1.42 \times 10^{-9}\ m^2 s^{-1}$. After three iterations, the optimum fit was obtained for $D^* = 2.875 \times 10^{-9}\ m^2 s^{-1}$. Figure 28 shows an excellent fit between measurements and the C_{RD} curve obtained from the SA1 solution. Some discrepancy is observed at early times, but at these low concentrations there is measurement uncertainty due to analytical errors.

In the second set of history-matching runs, linear equilibrium sorption was assumed, and both D^* and K_d were perturbed simultaneously. Their starting values were those at the end of the first history-matching set, i.e., $D^* = 2.875 \times 10^{-9}\ m^2 s^{-1}$ and $K_d = 5.2 \times 10^{-2}\ m^3 kg^{-1}$. After a total of 9 iterations, the objective function was minimized for $D^* = 1.671 \times 10^{-9}\ m^2 s^{-1}$ and $K_d = 2.465 \times 10^{-2}\ m^3 kg^{-1}$. The fit between the corresponding C_{RD} curve and the experimental observations is excellent. Although this curve appears to fit the data somewhat better than that from the first history-matching set, their differences are practically negligible.

In the third of history-matching runs, a linear kinetic sorption model was assumed, and D^* K_d and k were determined. The starting values of D^* and K_d were those at the end of the second history-matching set, and the initial $k = 10^{-4}\ s^{-1}$. The inversion of this set was far more difficult because of the larger number of perturbed parameters. After a total of 17 iterations, the objective function was minimized for $D^* = 2.00 \times 10^{-9}\ m^2 s^{-1}$, $K_d = 3.218 \times 10^{-2}\ m^3 kg^{-1}$, and $k = 3.06 \times 10^{-5}\ s^{-1}$. These parameters provide the best fit with the experimental data (lowest value of the objective function).

A review of Figure 28 points out the weaknesses of the conventional method of parameter estimation from through-diffusion experiments. Its empirical nature cannot be relied upon to provide accurate estimates. Additionally, the same experimental data were matched almost equally well with three curves representing different sorption models and involving different values of the pertinent parameters. The conventional approach limits measurements to the downstream reservoir (i.e., to C_{RD}), and is incapable of resolving the

ambiguities arising from non-unique solutions. These uncertainties could be overcome if a second data set, that of C_{RU}, were available.

The point is illustrated in Figure 29, which depicts the C_{RU} behavior corresponding to the C_{RD} curves of Figure 28. It is obvious that the four curves are easily distinguishable from each other. Had such a data set been available, it would have been possible to determine (a) the type of sorption (equilibrium or kinetic) and (b) the corresponding parameters with a far higher degree of certainty. The semi-analytical solution developed in this paper makes this possible.

It must be pointed out that Figure 29 also demonstrates another weakness of the conventional approach, namely the violation of the assumption of constant $C_U = C_{U0}$ for equation (61) to be valid. Because of technical difficulties, it is common practice to avoid replenishing the upstream reservoir to maintain a constant C_U, and to use only the first C_{RD} data for analysis. These data are inherently less accurate because of analytical errors at these low concentration levels. When larger data sets are used, it can be seen from Figure 29 that C_U exhibits a very significant decline that is controlled by the diffusion and sorption parameters. For the curve with the fixed $K_d = 5.2 \times 10^{-2}\ m^3 kg^{-1}$, C_{RU} declines very rapidly and reaches 0.54 at $t = 20$ days. Inclusion of the C_{RD} data points at the corresponding times contaminates the data set with substantial errors, as equation (61) is no longer valid. The semianalytical solution proposed here is general and suffers from no such shortcoming.

An important issue which must be addressed is that of increasing difficulty of history matching as the number of parameters to be determined increases. The availability of C_{RU} data set alleviates the problem, but if the history-matching technique is not sufficiently robust, parameter estimation may suffer from non-uniqueness. The history-matching method of *Thomas and Hellums* [1972] used in this analysis is based on the Gauss-Newton algorithm, and may be unstable in the inversion of the strongly non-linear problems of diffusion

discussed in this paper. In the author's experience, it is always possible to determine one parameter using this algorithm, and two parameters can be easily determined if the starting point is close to the solution. It is possible to determine three parameters only if the starting point is close to the solution, and it is not advisable to attempt the simultaneous determination of more than three parameters.

To address this problem, an existing inversion package *Finsterle* [1997] is currently being coupled with the semianalytical diffusion equation for automatic parameter estimation. This history-matching package includes the Levenberg-Marquardt algorithm and simulated annealing, and has been shown capable of determining simultaneously several parameters in extremely non-linear problems [*Finsterle and Persoff*, 1997].

7. Summary

In this paper semianalytical solutions to the problem of diffusion and sorption in diffusion cell experiments are developed. The PDE solved accounts for diffusion in the PM pores, surface diffusion, mass transfer between the mobile and immobile water fractions, linear sorption (equilibrium, kinetic or irreversible), and radioactive decay. Using Laplace transforms, analytical solutions are developed in the Laplace space. Direct inversion of these solutions to obtain a closed-form solution in time is not possible, thus the numerical inversion schemes of *Stehfest* [1970*a;b*] and of *De Hoog et al.* [1982] are employed. These semianalytical solutions make possible the analysis of data from diffusion experiments without suffering from the shortcomings and inaccuracies of the conventional empirical approach, which only uses information from the downstream reservoir (i.e., C_{RD}).

The semianalytical solutions are developed for the conditions of through-diffusion experiments, but it is shown that extension to reservoir-depletion and in-diffusion experiments is trivial, and is accomplished by setting the downstream reservoir volume $V_D = 0$ in the

solutions. The generality in the development of the solutions allows any length of the PM sample, and thus the equations can be used for scoping calculations in waste containment applications.

The semi-analytical solutions are verified under limit conditions, for which closed-form analytical solutions exist. The effects of various diffusion, sorption and geometric parameters on the solutions are investigated.

In through-diffusion experiments and under linear equilibrium sorption, diffusion is shown to increase with the pore diffusion coefficient. Increasing sorption shifts both the C_{RU} and C_{RD} curves downward (as less species mass remains in the liquid phase), and delays breakthrough in the downstream reservoir. In PMs which support surface diffusion exists, it is shown to account for practically all diffusion when sorption is strong, and its effects become more pronounced as sorption (i.e., the K_d) increases. Accounting for the mass transfer between the mobile and the immobile water fractions results in smaller R and, to a lesser extent, D^* values, and gives the appearance of lower sorption. Radioactive decay appears to have an effect if the radionuclide species has a short half life and the duration of the diffusion experiment is sufficiently long. The study of the effects of the cell geometry indicates the ability to selectively enhance the C_{RU} and C_{RD} signals by varying the absolute and relative sizes of V_U and/or V_D, and by adjusting A.

This study shows that the use of the semianalytical solutions has significant advantages over the conventional graphical approach because (a) it is not based on the often invalid assumption of constant upstream concentration $C_U = C_{U0}$, and (b) doubles the amount of data (by providing both the more sensitive C_{RU} and the C_{RD} measurements), from which to extract the pertinent diffusion and sorption parameters. Thus, a larger number of parameters can be determined with greater accuracy.

In the investigation of diffusion with linear kinetic sorption, an increasing k is shown to result in faster depletion in the upstream reservoir and slower breakthrough curves, and

increasing sorption amplifies these effects. Of particular interest is the effect of surface diffusion in diffusion with kinetically controlled sorption, which results in oscillatory C_{RD} behavior. In diffusion with irreversible sorption, the effect of K_L is that of a delay, or even elimination, of breakthrough.

A similar approach can be followed in the case of reservoir-depletion and/or in-diffusion, which is a simplified option of the through-diffusion case. This solution is used for scoping calculations of radionuclide fate and transport using data from the H-basin area of the Savannah River Site [*Moridis et al.*, 1996; *Hakem et al.*, 1997].

Finally, the semianalytical solution is coupled with the history-matching algorithm of *Thomas and Hellums* [1972] for the estimation of the diffusion and sorption parameters of shales, using previously published data [*McKinley and Swaminathan*, 1996]. In three sets of history matching runs, (a) D^* is obtained for a fixed K_d equal to that determined from batch experiments [*McKinley and Swaminathan*, 1996], (b) both D^* and K_d are simultaneously determined for a linear equilibrium sorption model, and (c) D^*, K_d and k are simultaneously determined for a linear kinetic sorption model. The excellent fits between observations and predictions based on the parameters from the three history-matching runs are in contrast with the significant deviations of the curve obtained using the parameters from the conventional analysis, which cannot be relied upon to provide accurate estimates.

These results indicate both the power and accuracy of the semianalytical solution for parameter estimation, as well as the ambiguities which stem from using only C_{RD} data, as the same experimental data were matched almost equally well with three curves representing different sorption models and involving different values of the pertinent parameters. An examination of the corresponding C_{RU} curves indicates that they are easily distinguishable from each other, and can resolve the ambiguities arising from non-unique solutions. The semi-analytical solution developed in this paper makes this possible.

Appendix A

Equating the change in the dissolved species mass in the upstream reservoir with the mass that crosses the $x = 0$ boundary and that lost due to radioactive decay, we have

$$\begin{aligned} -\int_0^t A\,\phi\,D_T \left(\frac{\partial C}{\partial x}\right)_{x=0} dt - \int_0^t A\,\phi\,D_F \left(\frac{\partial F}{\partial x}\right)_{x=0} dt \\ = V_U\,C_{U0} - V_U \left(C_U + \lambda \int_0^t C_U\,dt\right), \end{aligned} \tag{A1}$$

where all the terms are as previously defined. For simplicity, we consider the case of linear equilibrium sorption. Taking into account equations (18) and (21), the Laplace transform of (A1) yields after a simple manipulation

$$\alpha\,\frac{\eta_1}{\eta_2} + \beta = \frac{V_U\,C_{U0}}{s}\,\frac{1}{\eta_2}, \tag{A2}$$

where

$$\eta_1 = V_U\left(1 + \frac{\lambda}{s}\right) - \frac{D^*\,A\,\phi\,m}{s} \quad \text{and} \quad \eta_2 = V_U\left(1 + \frac{\lambda}{s}\right) + \frac{D^*\,A\,\phi\,m}{s}. \tag{A3}$$

Substituting α from equation (31) into (A2), β is determined from

$$\beta = \frac{V_U\,C_{U0}}{s}\,\frac{1}{\eta_2 + \gamma\,\eta_1\exp(-2m\,L)}. \tag{A4}$$

For linear kinetic and linear irreversible sorption, equation (A4) applies unchanged when the appropriate D^* and R^* expressions are used (see Sections 3.2 and 3.3).

Acknowledgments. This work was supported by the U.S. Department of Energy, Office of Environmental Management, Office of Technology Development, Subsurface Contamination Focus Area, under Contract No. DE-AC03-76SF00098. The author is particularly indebted to Dr. John Apps, whose deceptively simple and deviously devastating questions about the scientific implications of the findings were the source of considerable misery and

the cause for several revisions of the paper. Drs. Karsten Pruess, Chao Shan and Stefan Finsterle are thanked for their insightful review comments. Special thanks are extended to Dr. Marvin D. McKinley for making available to the author data from his diffusion experiments.

References

Bear, J., *Hydraulics of Groundwater*, McGraw-Hill, New York, 1979.

Berry, J. A., and K. A. Bond, Studies of the extent of surface diffusion in the migration of radionuclides through geological media, *Radiochimica Acta, 58/59*, 329-335, 1992.

Bradbury, M. H., D. Lever, and D. Kinsey, Aqueous phase diffusion in crystalline rocks, in *Scientific Basis for Nuclear Waste Management V*, vol. 11, pp. 569-578, Elsevier, New York, 1982.

Bradbury, M. H., A. Green, D. Lever, and I. G. Stephen, Diffusion and permeability based sorption measurements in sandstone, anhydrite and upper magnesian limestone samples, *Report AERE-R 11995*, UKAEA, Harwell Laboratory, Oxfordshire, 1986.

Cook, A. J., A desk study of surface diffusion and mass transport in clay, *Report WE/88/34*, Commission of the European Communities, Directorate-General, Sciences Research and Development, Louxemburg, 1989.

Crank, J., *The Mathematics of Diffusion*, 2nd ed., Oxford University Press, New York, 1975.

Crump, K. S., Numerical inversion of Laplace transforms using a Fourier Series approximation, *J. Assoc. Comput. Mach., 23*(1), 89-96, 1976.

De Hoog, F. R., J. H. Knight, and A. N. Stokes, An improved method for numerical inversion of Laplace transforms, *SIAM J. Sci. Stat. Comput., 3*(3), 357-366, 1982.

de Marsily, G., *Quantitative Hydrogeology*, Academic Press, San Diego, 1986.

Finsterle, S., and P. Persoff, Determining permeability of tight rock samples using inverse modeling, *Water Resour. Res., 33*(8), 1803-1811, 1997.

Finsterle, S., ITOUGH2 user's guide, Version 3.1, *Report LBNL-40400*, Lawrence Berkeley National Laboratory, Berkeley, Calif., 1997.

Fisher, G. W., and A. C. Lasaga, Irreversible thermodynamics in petrology, in *Reviews in Minerology, Vol. 8: Kinetics of Geochemical Processes*, pp. 171-207, Mineralogical Society of America, Washington, D.C., 1981.

Hakem, N., I. Al-Mahamid, J. Apps, and G. Moridis, Sorption of Cs-137 and Sr-88 on Savannah River soils impregnated with colloidal silica, in *Proceedings,* International Containment Technology Conference, February 9-12, 1997, St. Petersburg, Florids, Pg. 652-657, 1997 (also *Report LBNL-39498*, Lawrence Berkeley National Laboratory, Berkeley, Calif.).

Harada, M., P. L. Chambré, M. Foglia, K. Higashi, F. Iwamoto, D. Leung, D. H. Pigford, and D. Ting, Migration of radionuclides through sorbing media, *Report LBL-10500*, Lawrence Berkeley Laboratory, Berkeley, Calif., 1980.

Jahnke, F. M., Electrolyte diffusion in montmorillonite engineered barriers, Ph.D. dissertation, Univ. of Calif., Berkeley, 1986.

Jahnke, F. M., and C. J. Radke, Electrolyte diffusion in compacted montmorillonite engineered barriers, in *Coupled Processes Associated With Nuclear Waste Repositories*, pp. 287-297, Academic Press, Orlando, 1987.

Jensen, D. J., and C. J. Radke, Cation diffusion through compacted sodium montmorillonite at elevated temperature, *J. Soil Sci., 39*, 53-64, 1988.

Kirchner, G., G. Nageldinger, and R. Wellner, Modified diffusion technique for studying nonlinear and kinetic sorption and desorption processes, *Radiochimica Acta, 74*, 189-192, 1996.

Lever, D.A., Some notes on experiments measuring diffusion of sorbed nuclides through porous media, *Report AERE-R 12321*, UKAEA, Harwell Laboratory, Oxfordshire, 1986.

McKinley, M. D., and S. Swaminathan, Diffusion and sorption of lead and cadmium ions in Gulf Coast shales, in *Deep Injection Disposal of Hazardous and Industrial Waste*, pp. 529-551, Academic Press, San Diego, 1996.

Moridis, G. J., Alternative formulations of the Laplace Transform Boundary Element (LTBE) numerical method for the solution of diffusion-type equations, in *Boundary Element Technology VII*, pp. 815-833, Computational Mechanics Publications, Boston, and Elsevier Applied Science, New York, 1992*a*.

Moridis, G. J., Evaluation of numerical inversion algorithms in Laplace-transform based numerical methods for the solution of the equations of flow and transport in porous media (abstract), *EOS Trans. AGU, 73*(14), 123, 1992*b*.

Moridis, G. J., Y.-S. Wu, and K. Pruess, EOS9nT: A TOUGH2 module for flow and solute/colloid transport, *Report LBNL-41639*, Lawrence Berkeley National Laboratory, Berkeley, Calif., 1998.

Moridis, G. J., and D. L. Reddell, The Laplace Transform Finite Difference (LTFD) method for simulation of flow through porous media, *Water Resour. Res., 27*(8), 1873-1884, 1991.

Moridis, G. J., P. Persoff, J. Apps, A. James, C. Oldenburg, A. McGrath, B. Freifeld, L. Myer, L. Pellerin, and K. Pruess, A design study for the isolation of the 281-3H retention basin at the Savannah River Site using the Viscous Barrier Technology, *Report LBNL-38920*, Lawrence Berkeley National Laboratory, Berkeley, Calif., 1996.

Muurinen, A., P. Penttilä-Hiltunen, and K. Clusheimo, Diffusion of chloride and uranium in compacted sodium bentonite, in *Scientific Basis for Nuclear Waste Management V*, vol. 18, pp. 743-748, Elsevier, New York, 1989.

Oldenburg, C., and K. Pruess, Dispersive transport dynamics in a strongly coupled groundwater-brine flow system, *Water Resour. Res., 31*(2), 289-302, 1995.

Ortoleva, P. J., *Geochemical Self-Organization*, Oxford University Press, New York, 1994.

Pigford, D. H., P. L. Chambré, M. Albert, M. Foglia, M. Harada, F. Iwamoto, T. Kanki, D. Leung, S. Masuda, S. Muraoka, and D. Ting, Migration of radionuclides through sorbing media, Analytical solutions, *Report LBL-11616*, Lawrence Berkeley Laboratory, Berkeley, Calif., 1980.

Pruess, K., TOUGH2 - A general-purpose numerical simulator for multiphase fluid and heat flow, *Report LBL-29400*, Lawrence Berkeley National Laboratory, Berkeley, Calif., 1991.

Put, M. J., and P. N. Henrion, An improved method to evaluate radionuclide migration model parameters from flow-through diffusion tests in reconsolidated clay plugs, *Radiochimica Acta, 44/45*, 343-350, 1988.

Shackelford, C. D., Laboratory diffusion testing for waste disposal - A review, *J. Contam. Hydrol., 7*, 177-189, 1991.

Skagius, K., and I. Neretnieks, Porosities and diffusivities of some nonsorbing species in crystalline rocks, *Water Resour. Res., 22*(3), 389-398, 1986*a*.

Skagius, K., and I. Neretnieks, Diffusivity measurements and electrical resistivity measurements in rock samples under mechanical stress, *Water Resour. Res., 22*(4), 570-580, 1986*b*.

Skagius, K., and I. Neretnieks, Measurements of cesium and strontium diffusion in biotite gneiss, *Water Resour. Res., 24*(1), 75-84, 1988.

Smith, P. A., Modeling a diffusion-sorption experiment by linear and nonlinear sorption isotherms, *Nucl. Technol., 92*, 363-372, 1990.

Stehfest, H., Algorithm 368, Numerical inversion of Laplace transforms, *J. ACM, 13*(1), 47-49, 1970*a*.

Stehfest, H., Algorithm 368, Remark on algorithm 368 [D5], Numerical inversion of Laplace transforms, *J. ACM, 13*(1), 56, 1970*b*.

Thomas, L. K., and L. J. Hellums, A nonlinear automatic history matching technique for

reservoir simulation models, *SPE Trans., 253*, 106-112, 1972 (SPE Paper 3475).

Torstenfelt, B., Migration of the fission products strontium, technetium, iodine and cesium in clay, *Radiochimica Acta, 39*, 97-104, 1986.

Triay, I. R., A. Meijer, J. L. Conca, K. S. Kung, R. S. Rundberg, and E. A. Strietelmeier, Summary and synthesis report on radionuclide retardation for the Yucca Mountain Site characterization project, *Milestone Report 3784, MOL.19961231.0099*, Chemical Science and Technology Division, Los Alamos National Laboratory, Los Alamos, New Mexico, 1996.

van Genuchten, M. D., A closed-form equation for predicting the hydraulic conductivity of unsaturated soils, *Soil Sci. Soc. Am. J., 44*, 892-898, 1980.

Wen, R., H. Gao, X. Wang, and Y. Liu, Diffusion of fission fragment nuclides in granite, *Radiochimica Acta, 76*, 137-142, 1997.

Table 1. Standard parameters in the examples of the semianalytical solution

Parameter	Value	Parameter	Value
V_U	$2 \times 10^{-3}\ m^3$	V_D	$2 \times 10^{-3}\ m^3$
A	$10^{-2}\ m^2$	L	$10^{-2}\ m$
ϕ	0.35	ρ	$2600\ kgm^{-3}$
$\tau_p = \tau_i = \tau_s$	0.1	S_r	0.0
λ	$0\ s^{-1}$	D_0	$10^{-9}\ m^2s^{-1}$
$D_T = D^*$	$10^{-10}\ m^2s^{-1}$	D_s	$0\ m^2s^{-1}$
K_d	$4.14 \times 10^{-4}\ m^3kg^{-1}$	R^*	3
K_i	1	K_L	$0\ m^3kg^{-1}s^{-1}$
k	$0\ s^{-1}$	δ	1
M_H	20	E_R	10^{-9}
T	$t = t_{ob}$	μ	0

Table 2. Fixed parameters in the history-matching example

Parameter	Value	Parameter	Value
V_U	$4.906 \times 10^{-3}\ m^3$	V_D	$2.76 \times 10^{-3}\ m^3$
A	$7.854 \times 10^{-3}\ m^2$	L	$10^{-2}\ m$
ϕ	0.41	ρ	$2600\ kgm^{-3}$
$\tau_p = \tau_i = \tau_s$	1	S_r	0.0
λ	$0\ s^{-1}$	$D_T = D^*$	D_0
D_s	$0\ m^2s^{-1}$	K_i	1
K_L	$0\ m^3kg^{-1}s^{-1}$	δ	1
M_H	20	E_R	10^{-9}
T	$t = t_{ob}$	μ	0

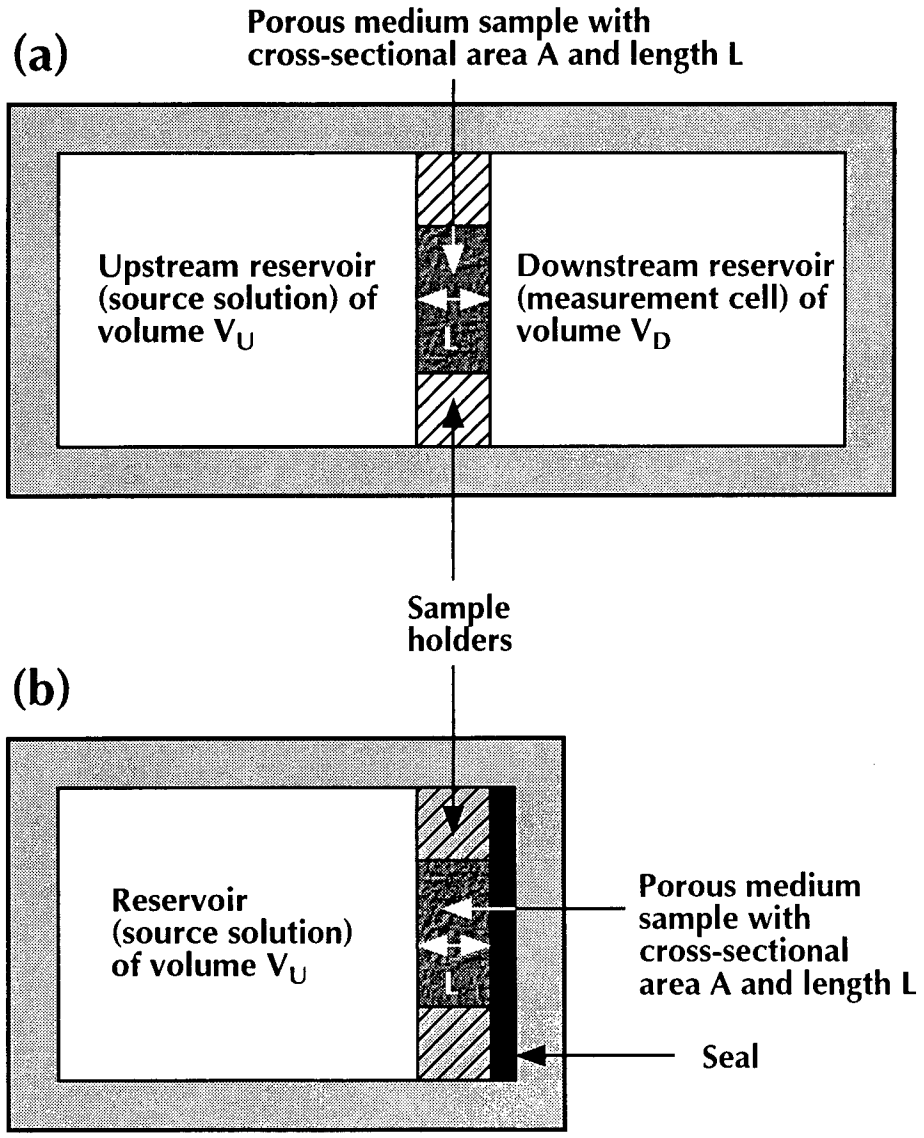

Figure 1. Diffusion cells for (a) through-diffusion experiments and (b) reservoir-depletion and/or in-diffusion studies.

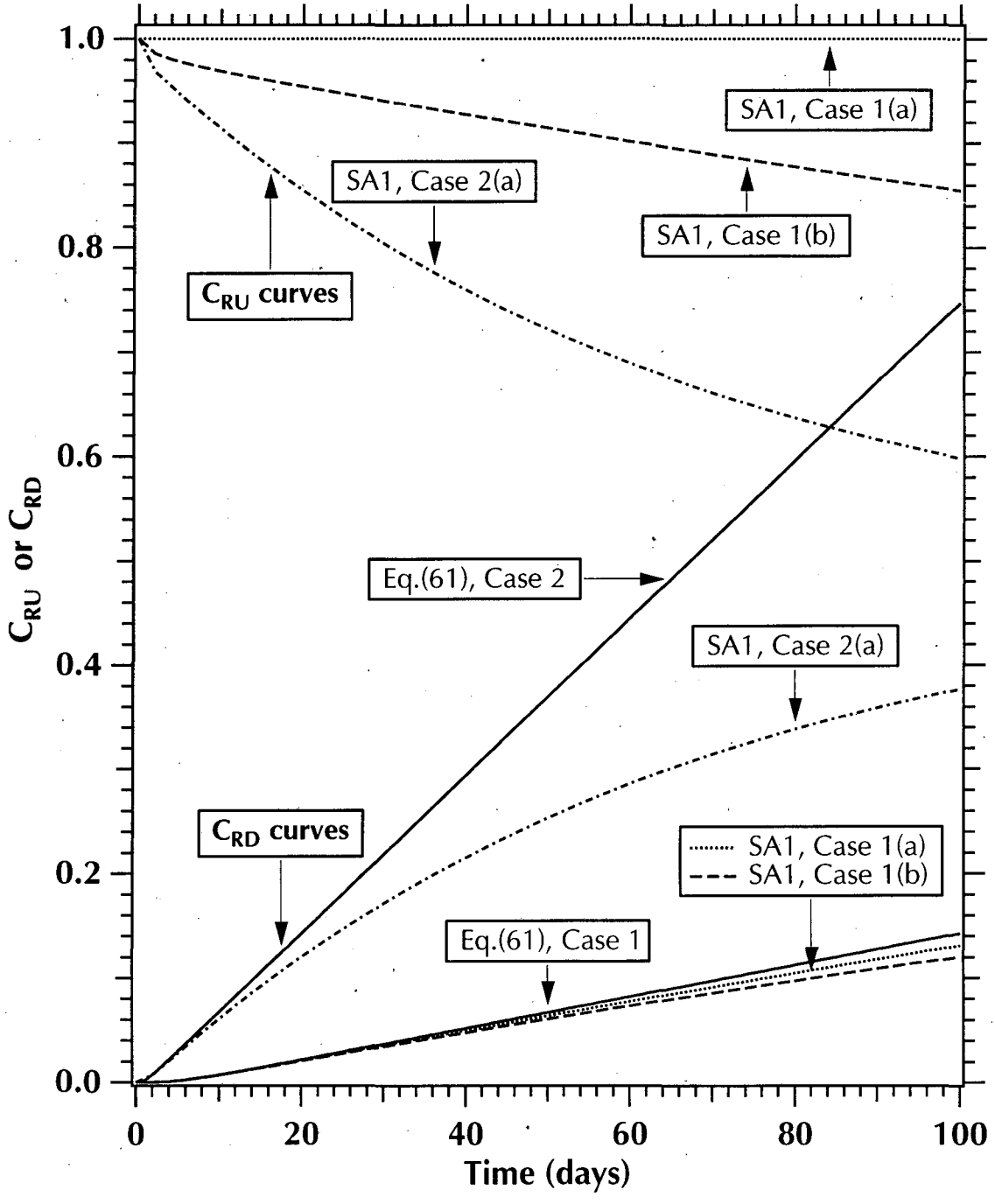

Figure 2. Comparison of the SA1 solutions of C_{RD} to the approximate analytical solutions of equation (61) [*Crank*, 1975]. The corresponding SA1 predictions of C_{RU} are also shown.

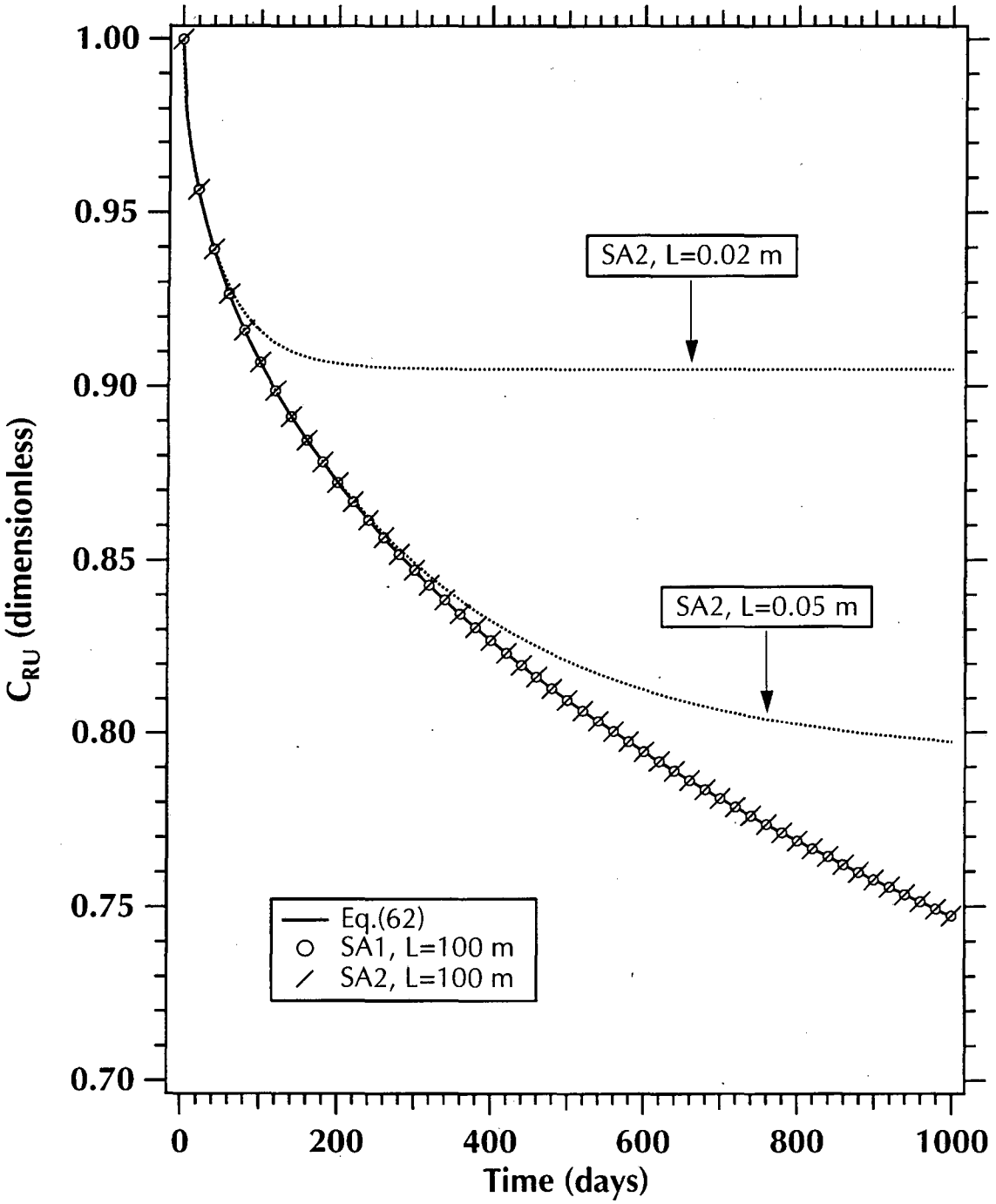

Figure 3. Comparison of the analytical solution [*Lever*, 1986] to (a) the SA1 solution for $L = 100\ m$, (b) the SA2 solution for $L = 100\ m$ and (c) the SA2 solutions for $L = 100\ m$, $L = 0.05\ m$, and $L = 0.02\ m$.

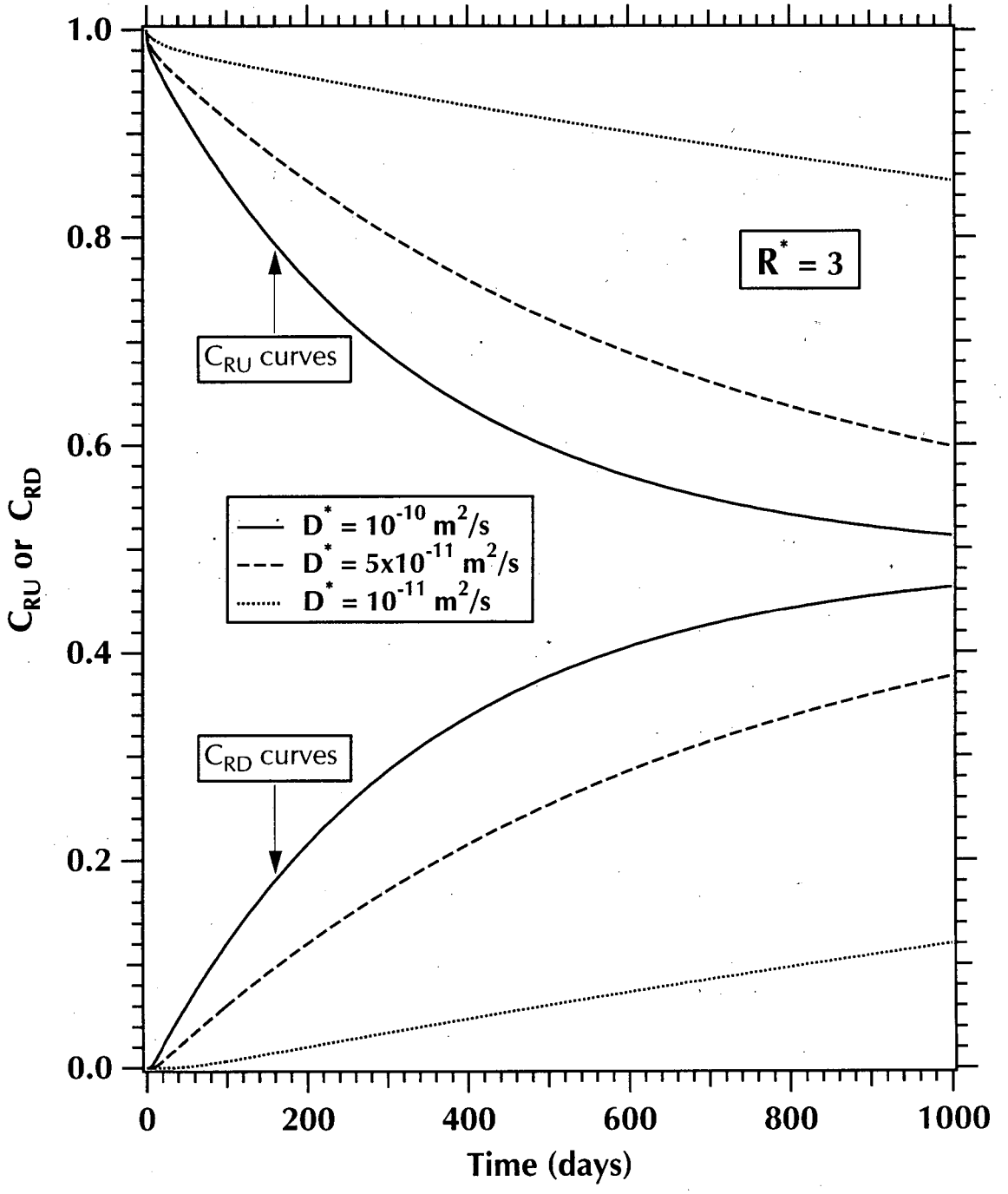

Figure 4. Effect of D^* on the C_{RU} and C_{RD} solutions for $R^* = 3$.

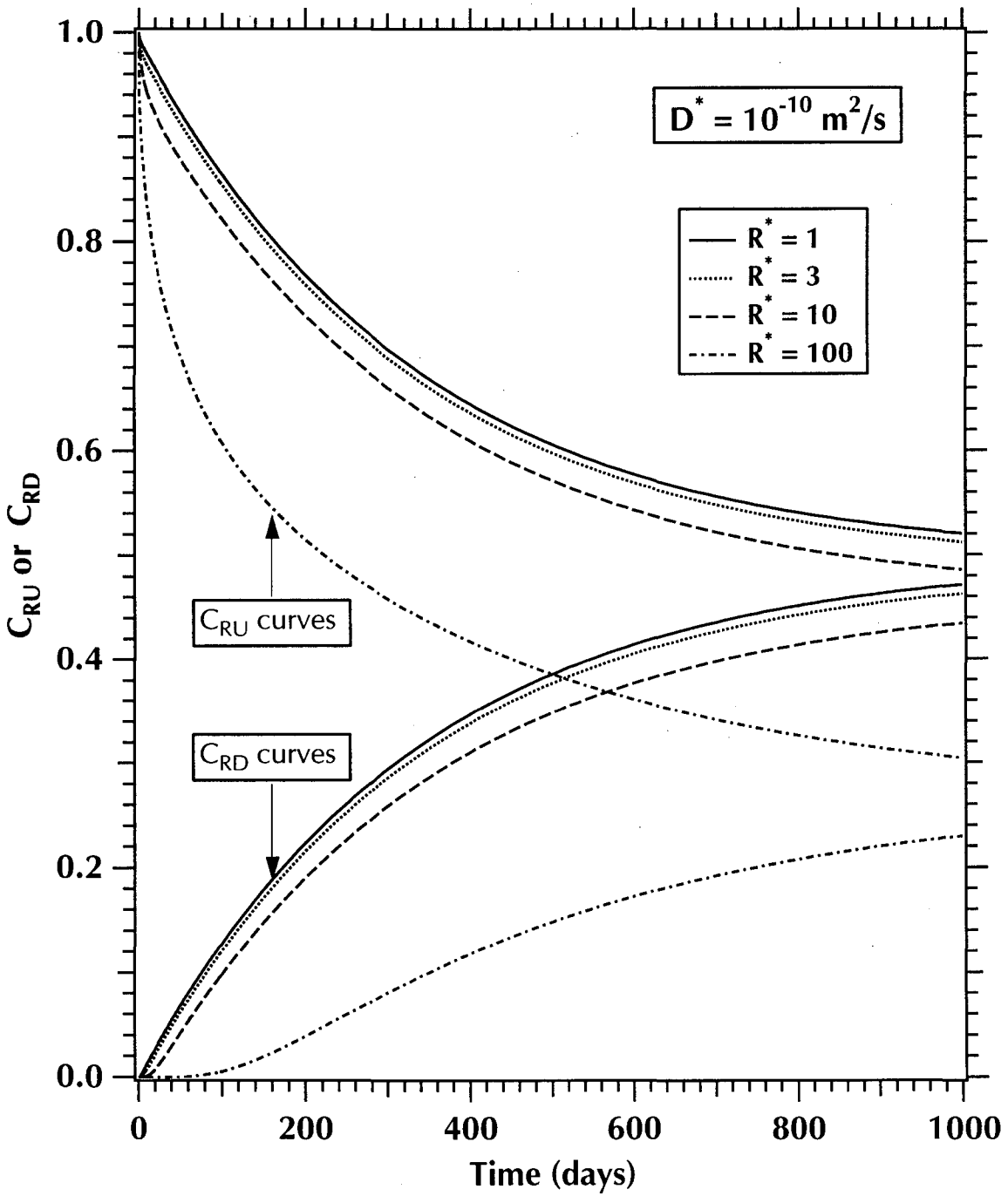

Figure 5. Effect of sorption (variable R^*) on the C_{RU} and C_{RD} solutions for $D^* = 10^{-10}$ m^2/s.

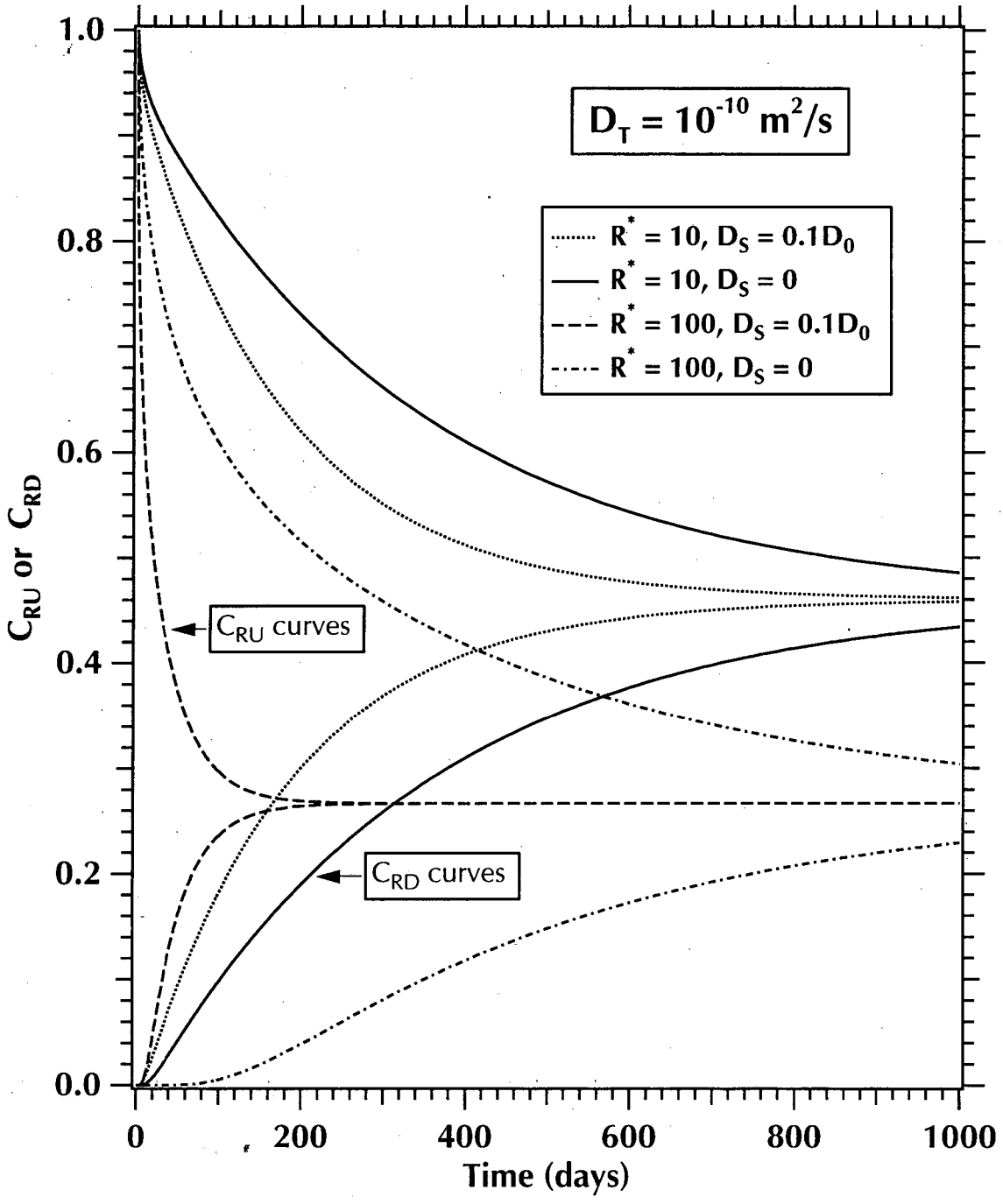

Figure 6. Effect of surface diffusion on the C_{RU} and C_{RD} solutions for two different R^* values.

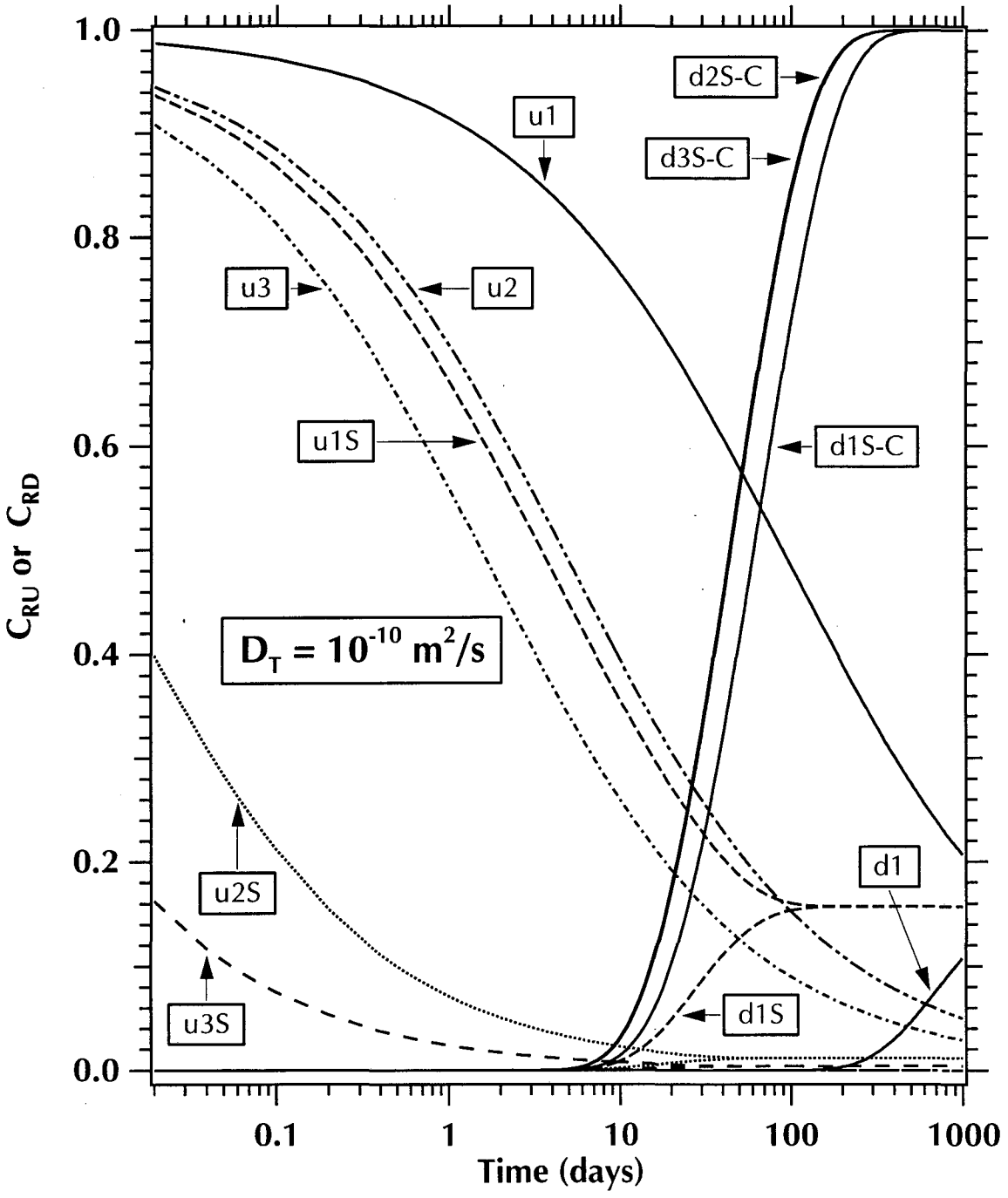

Figure 7. C_{RU} and C_{RD} behavior under conditions of very strong sorption and surface diffusion (1: $R^* = 250$, 2: $R^* = 4829$, 3: $R^* = 14486$, u: upstream, d: downstream, S: surface diffusion, C: conventional technique).

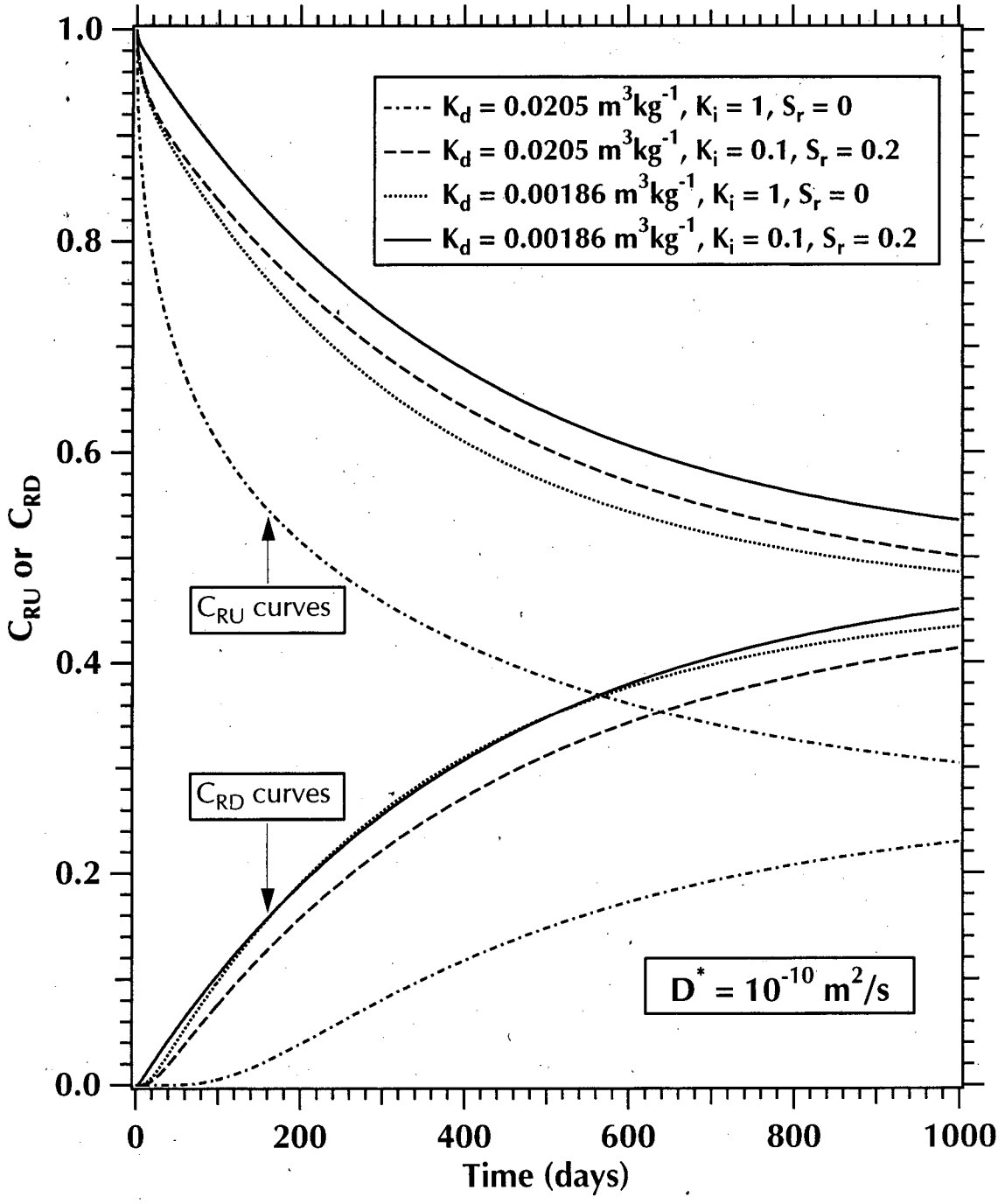

Figure 8. Effect of mass transfer between the mobile and immobile water fractions on the C_{RU} and C_{RD} solutions.

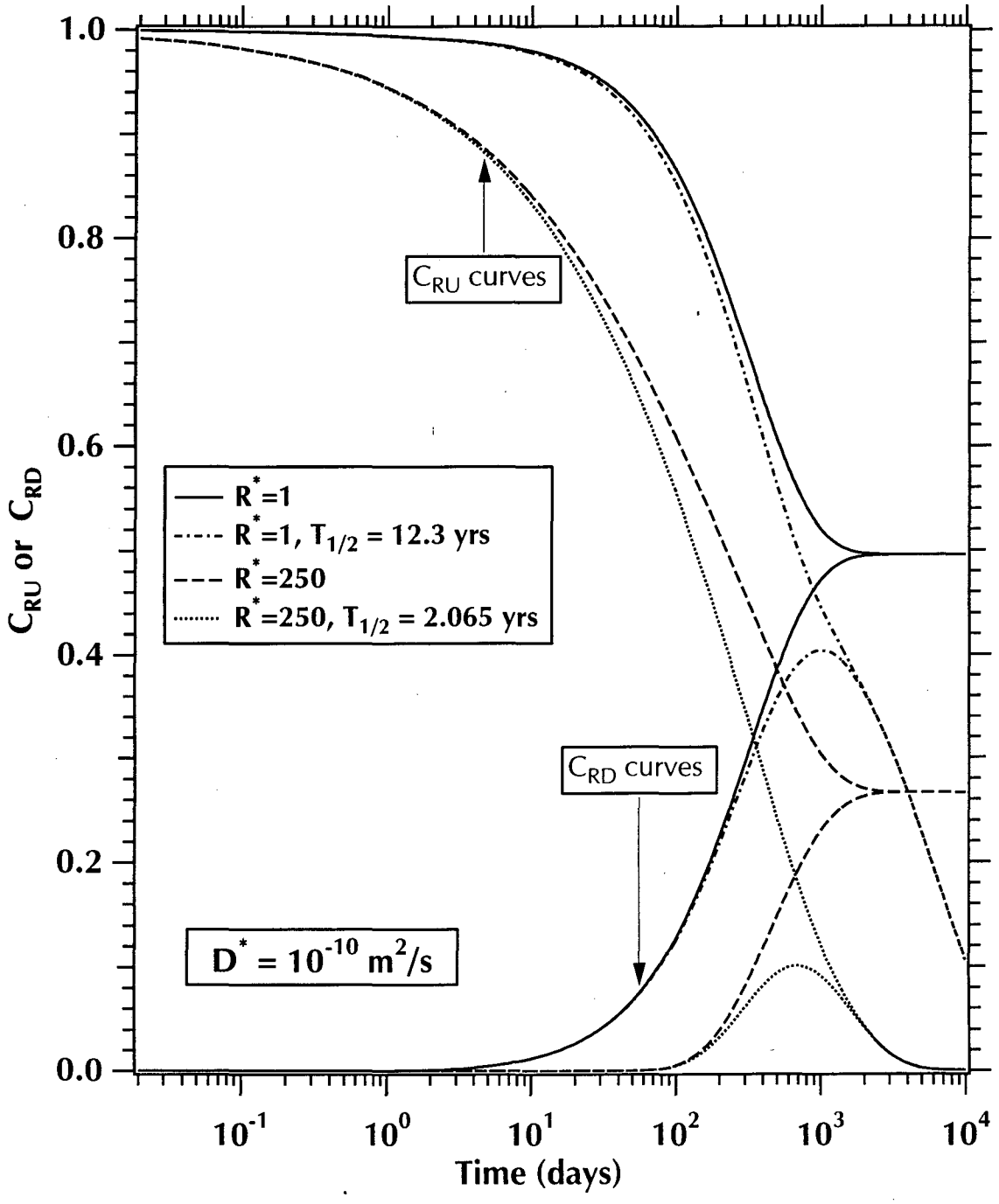

Figure 9. Effect of radioactive decay on the C_{RU} and C_{RD} solutions for (a) a non-sorbing ($R = 1$) species with $T_{1/2} = 12.32$ yrs (^{3}H) and (b) a strongly sorbing ($R^* = 250$) species with $T_{1/2} = 2.065$ yrs (^{134}Cs).

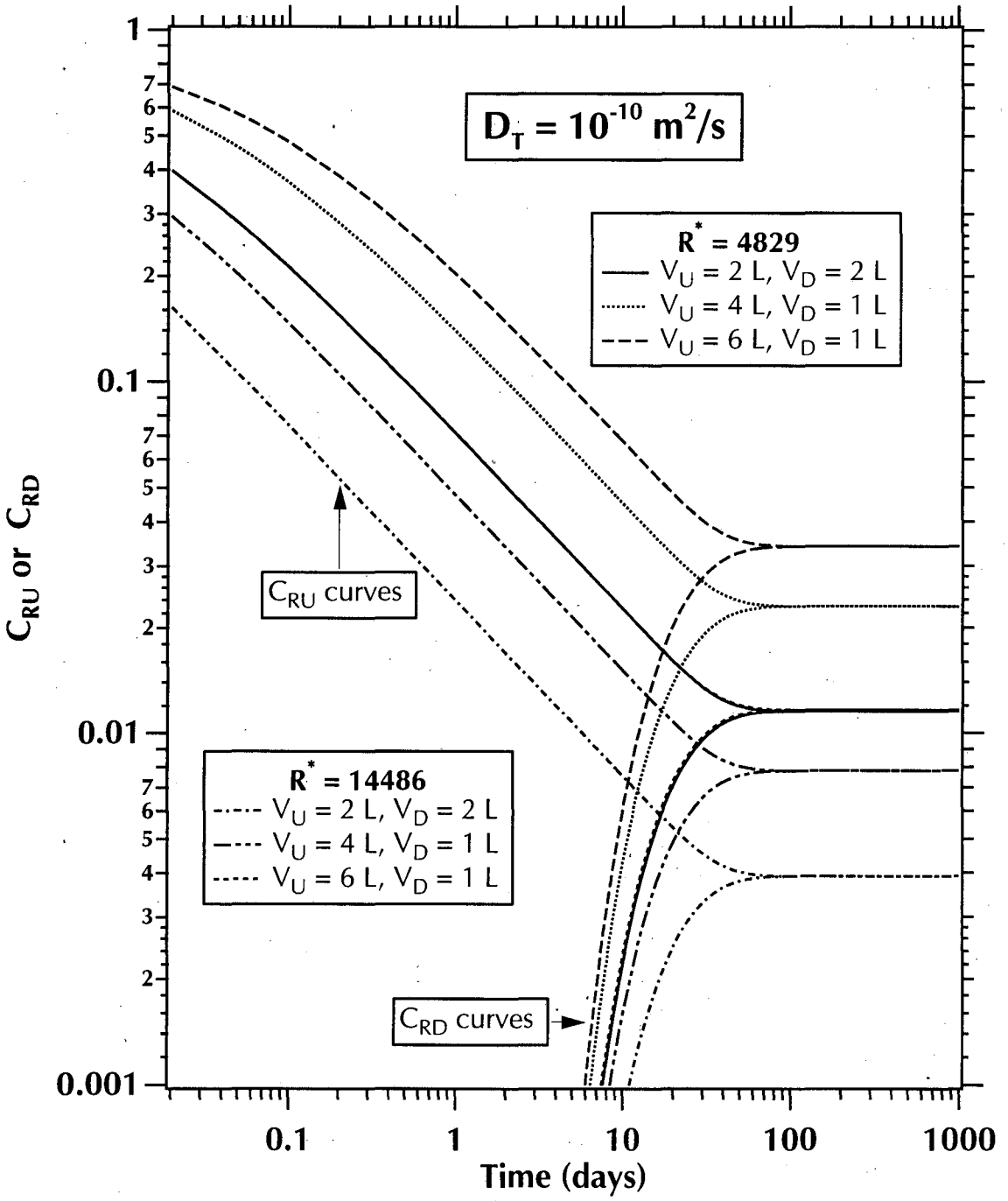

Figure 10. Effect of the size of V_U and V_D on the C_{RU} and C_{RD} solutions in the case of strong sorption with surface diffusion.

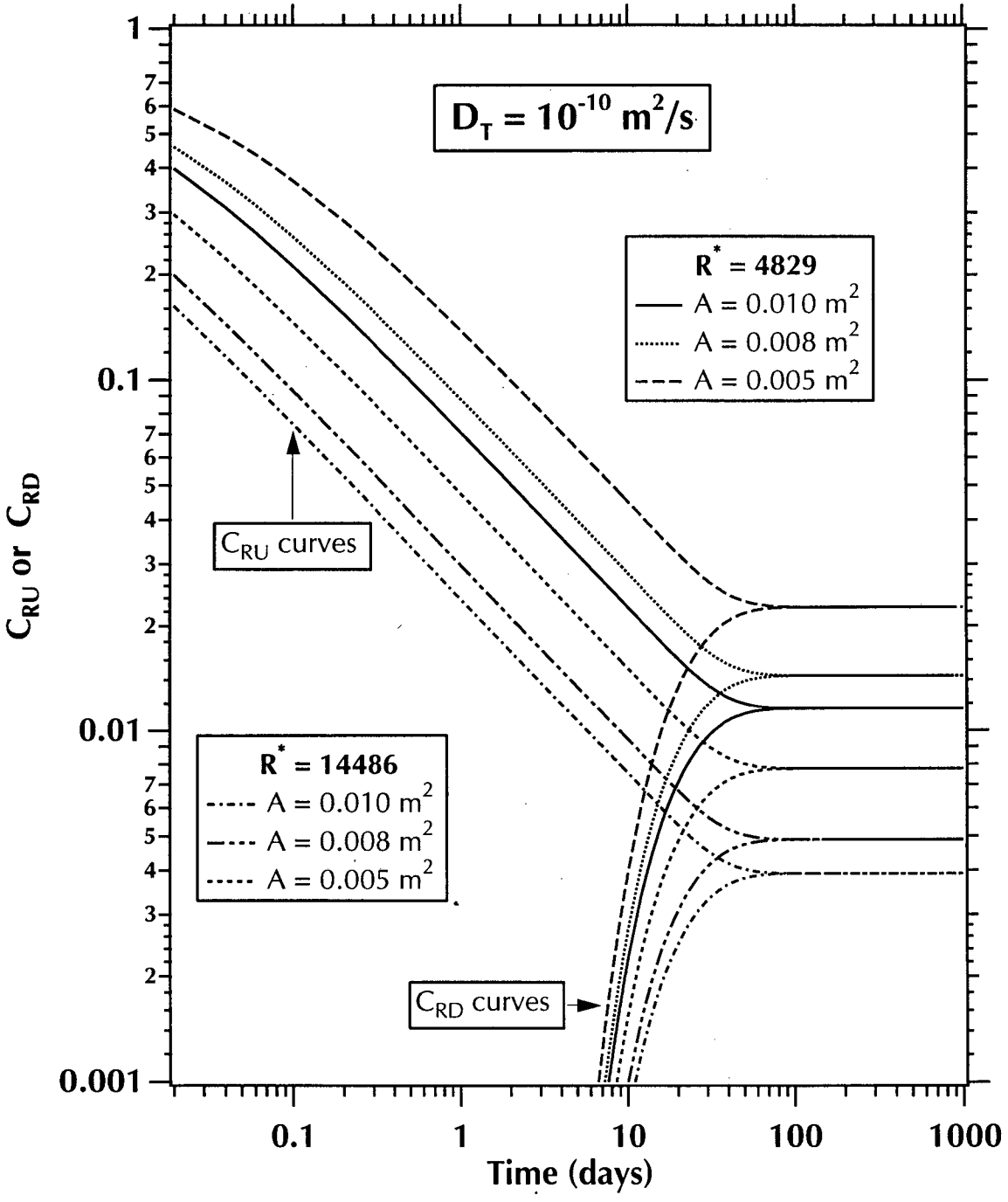

Figure 11. Effect of the size of A on the C_{RU} and C_{RD} solutions in the case of strong sorption with surface diffusion.

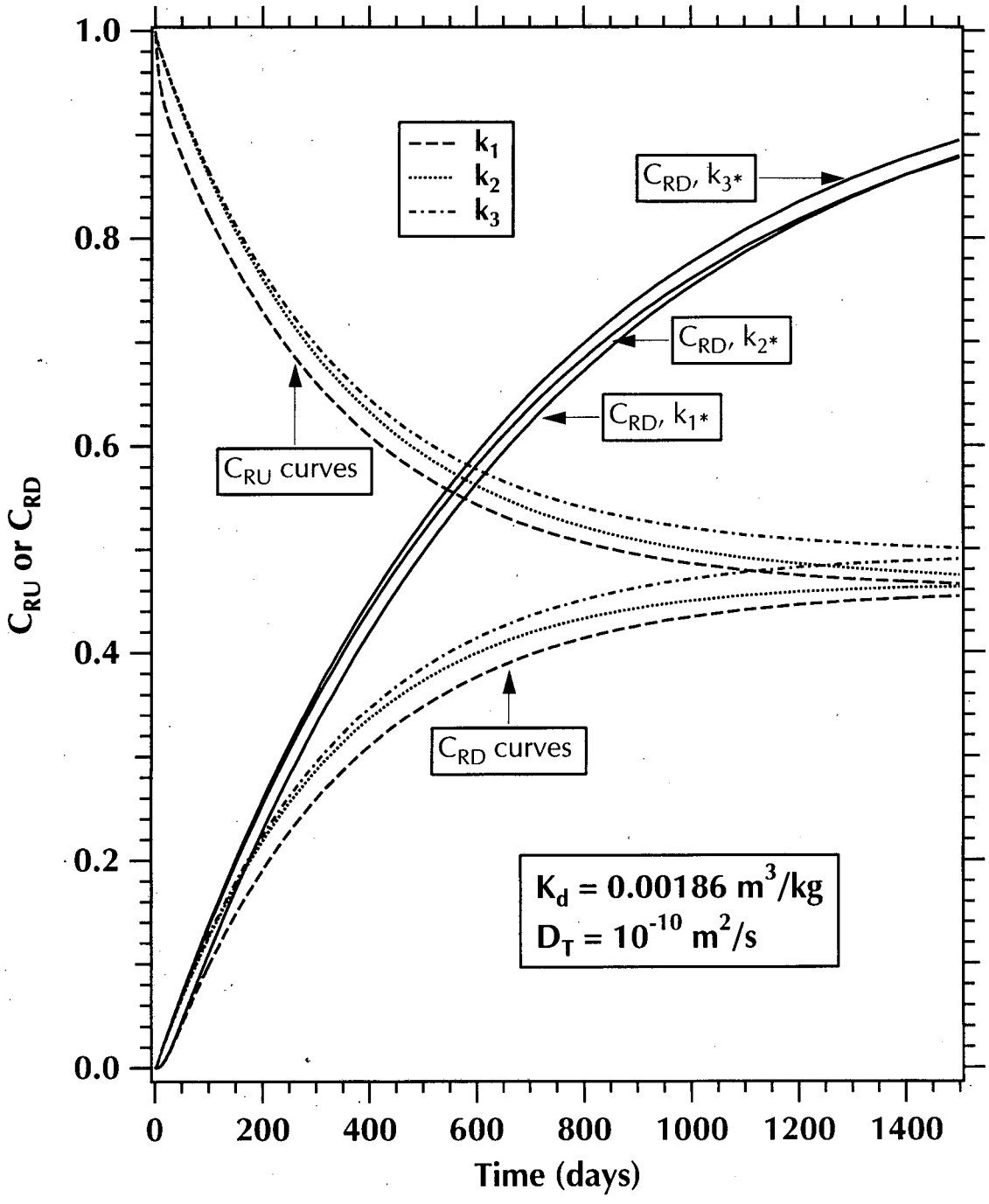

Figure 12. Effect of the kinetic constant k on the C_{RU} and C_{RD} solutions in a PM with a $K_d = 1.8639 \times 10^{-3}\ m^3 kg^{-1}$ ($k_1 = 10^{-5}\ s^{-1}$, $k_2 = 10^{-8}\ s^{-1}$, $k_3 = 10^{-10}\ s^{-1}$).

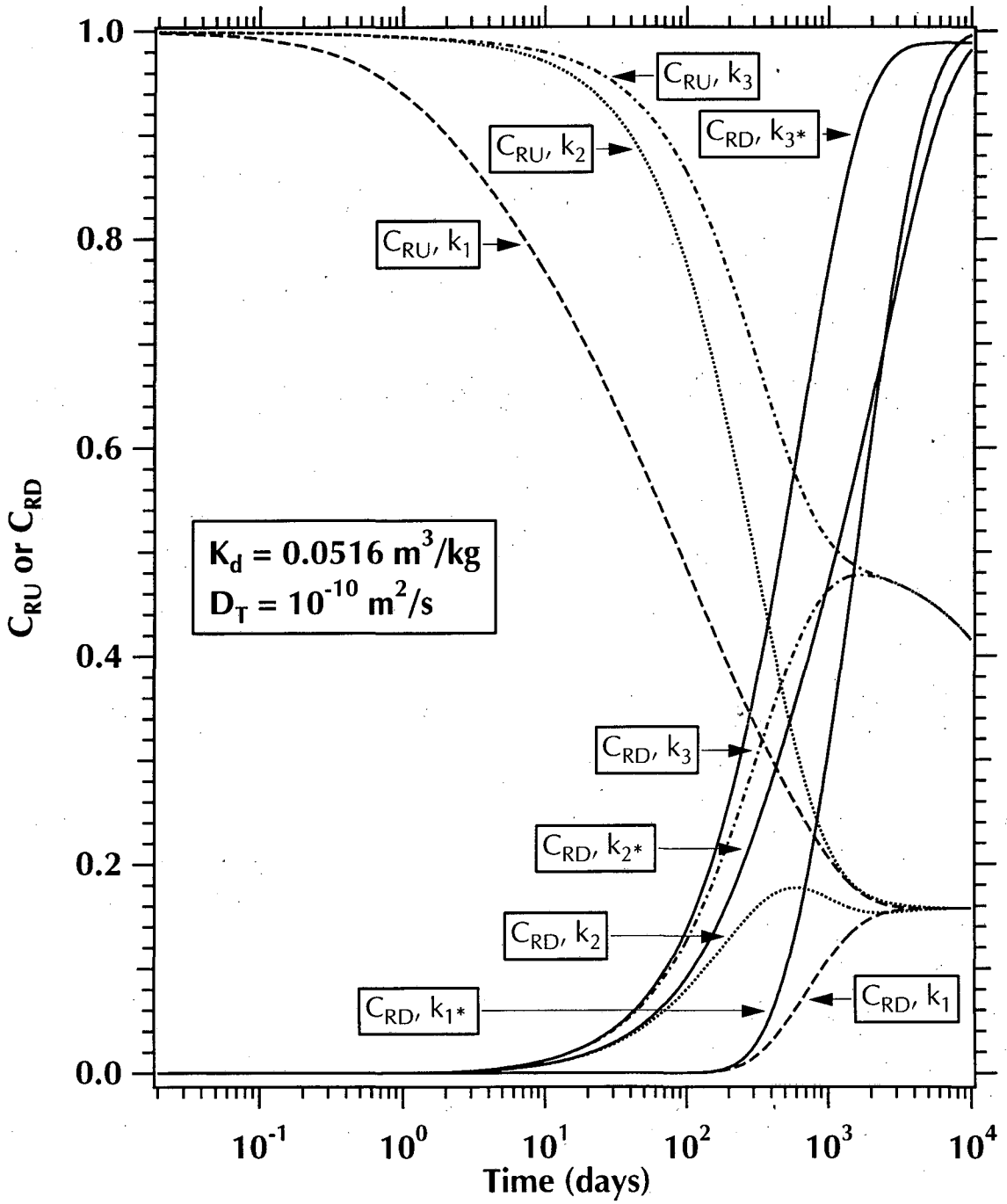

Figure 13. Effect of the kinetic constant k on the C_{RU} and C_{RD} solutions in a PM with a $K_d = 5.1568 \times 10^{-2}\ m^3 kg^{-1}$ (k_1, k_2, k_3 as in Figure 12).

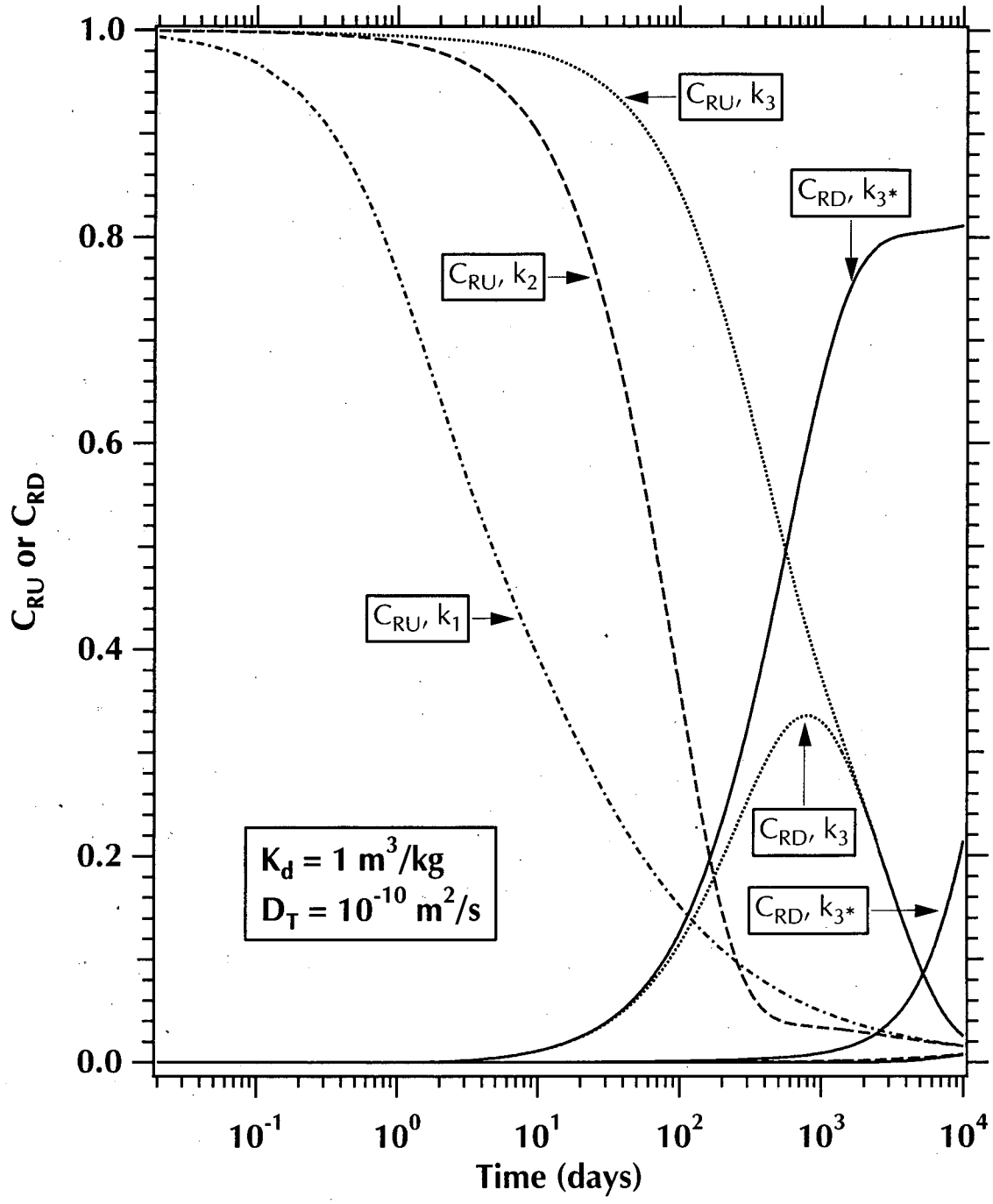

Figure 14. Effect of the kinetic constant k on the C_{RU} and C_{RD} solutions in a PM with a $K_d = 1\ m^3 kg^{-1}$ (k_1, k_2, k_3 as in Figure 12).

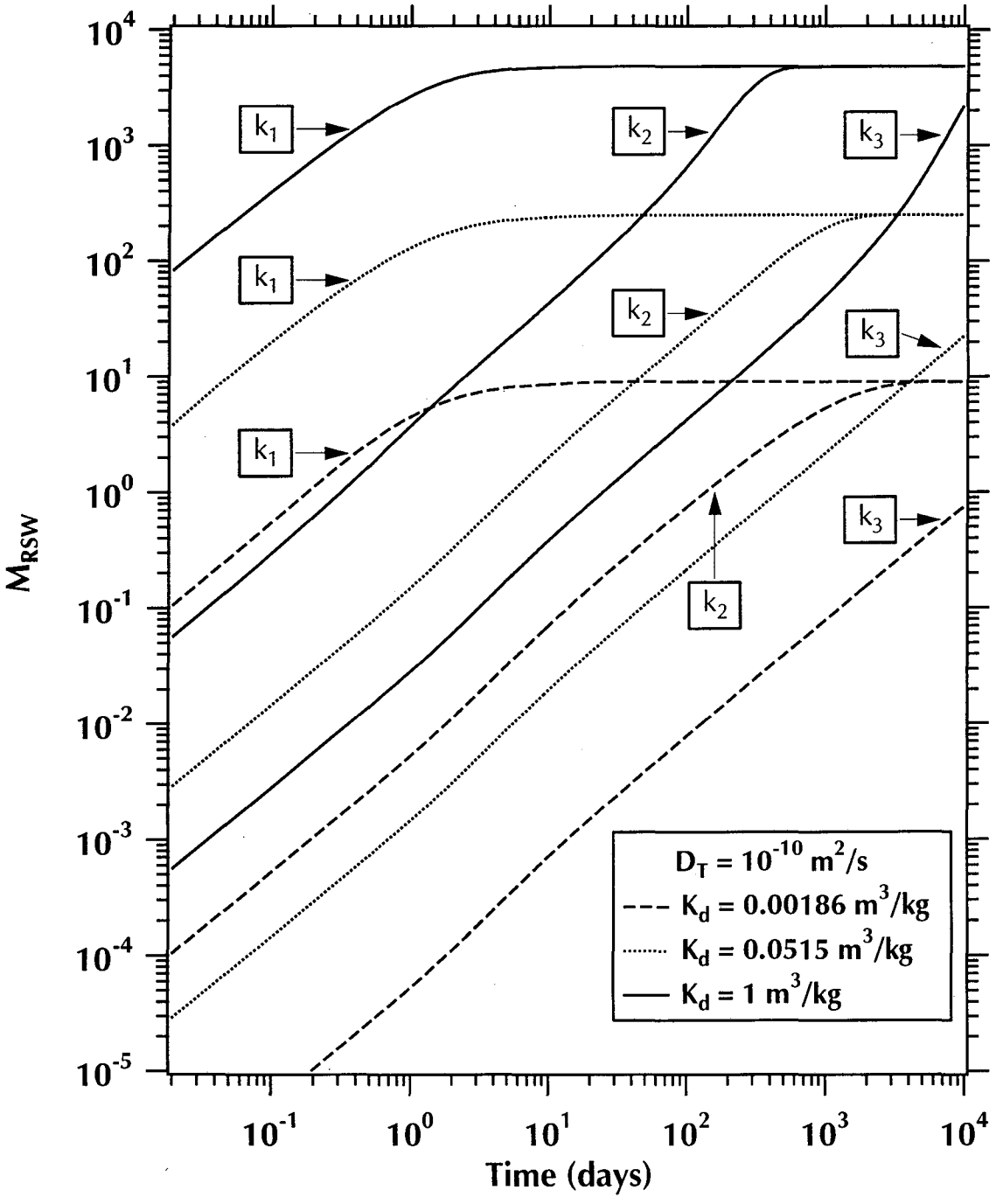

Figure 15. Evolution of the mass ratio $M_{RSW} = m_S/m_w$ over time for the combination of K_d and k of Figures 12 through 14.

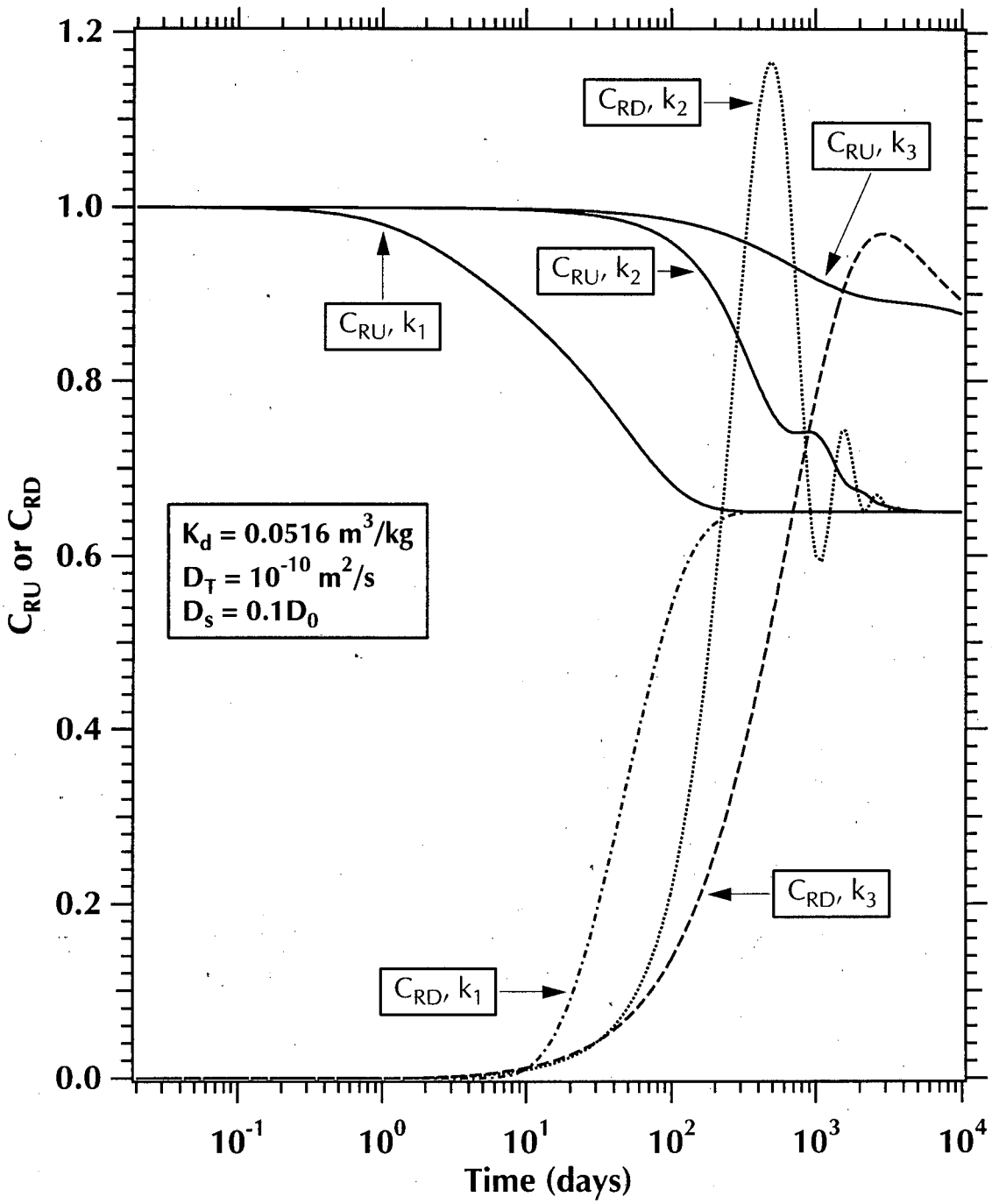

Figure 16. Effect of the surface diffusion $D_s = 0.1\,D_0$ on the C_{RU} and C_{RD} solutions in a PM with a $K_d = 5.1568 \times 10^{-2}\ m^3 kg^{-1}$ (k_1, k_2, k_3 as in Figure 12).

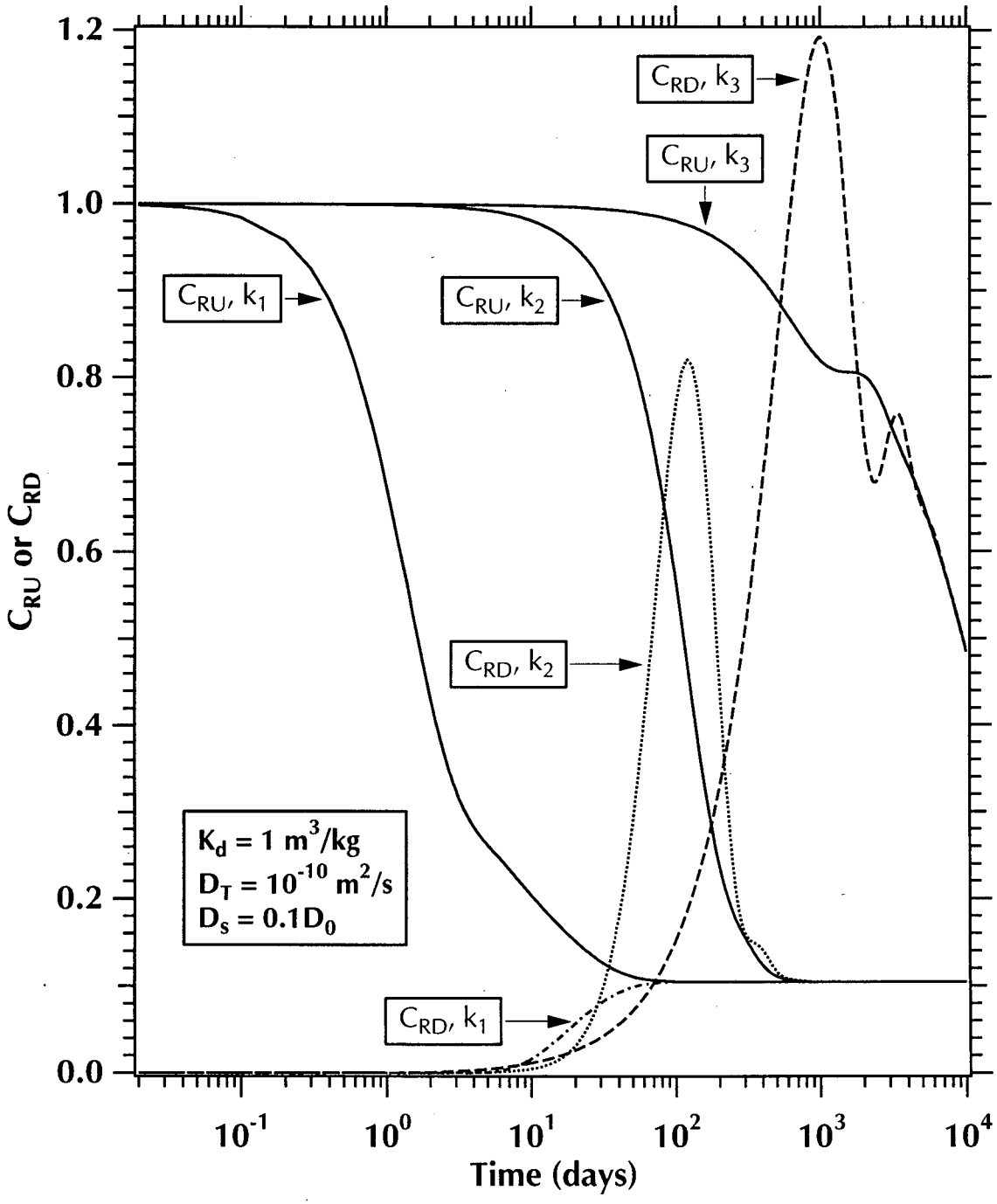

Figure 17. Effect of the surface diffusion $D_s = 0.1\,D_0$ on the C_{RU} and C_{RD} solutions in a PM with a $K_d = 1\ m^3 kg^{-1}$ (k_1, k_2, k_3 as in Figure 12).

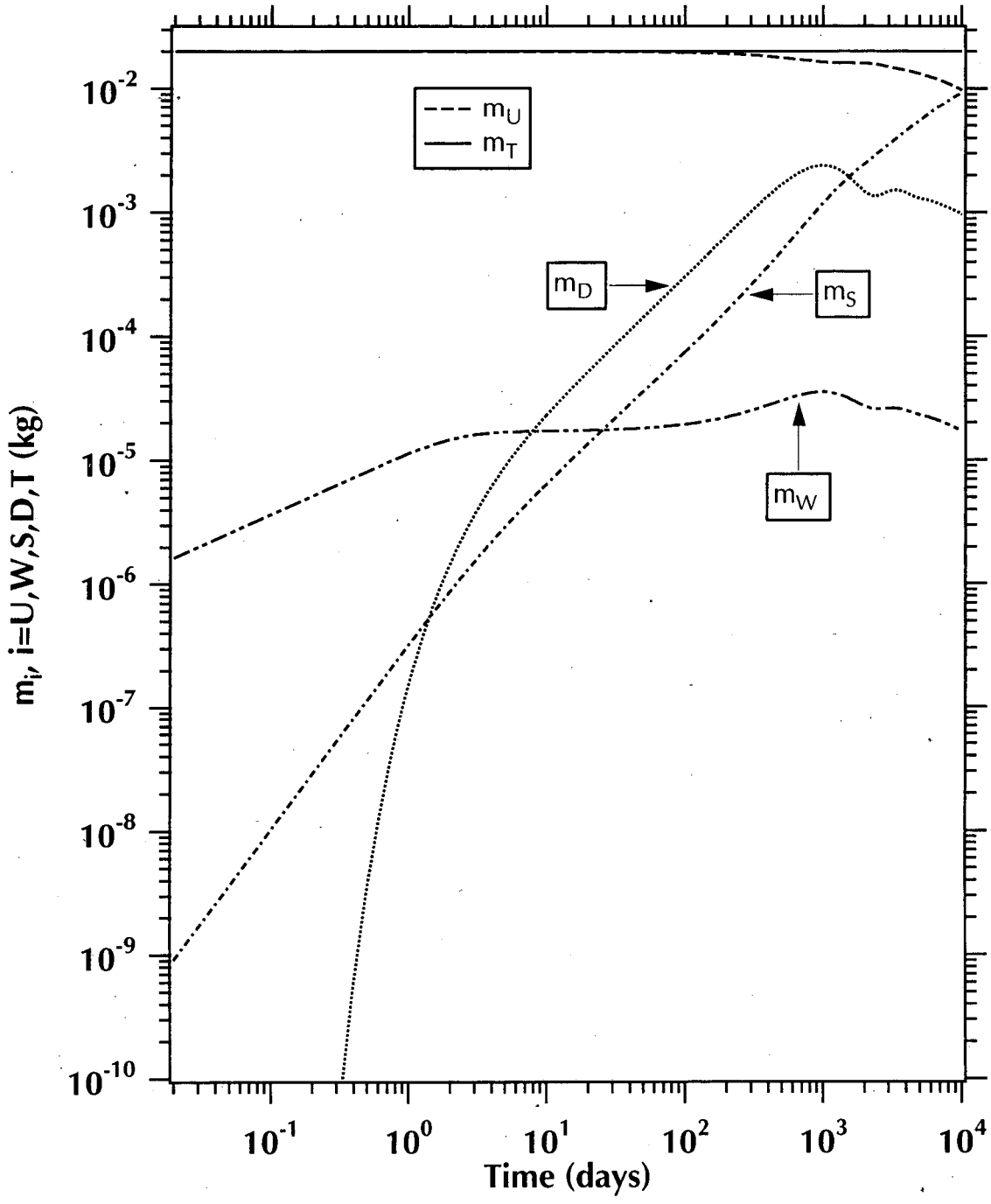

Figure 18. Mass of the dissolved species in the various components of the diffusion cell system (i.e., m_U, m_W, m_S, m_D, m_T) under the conditions of the study for $k = k_3$ in Figure 17.

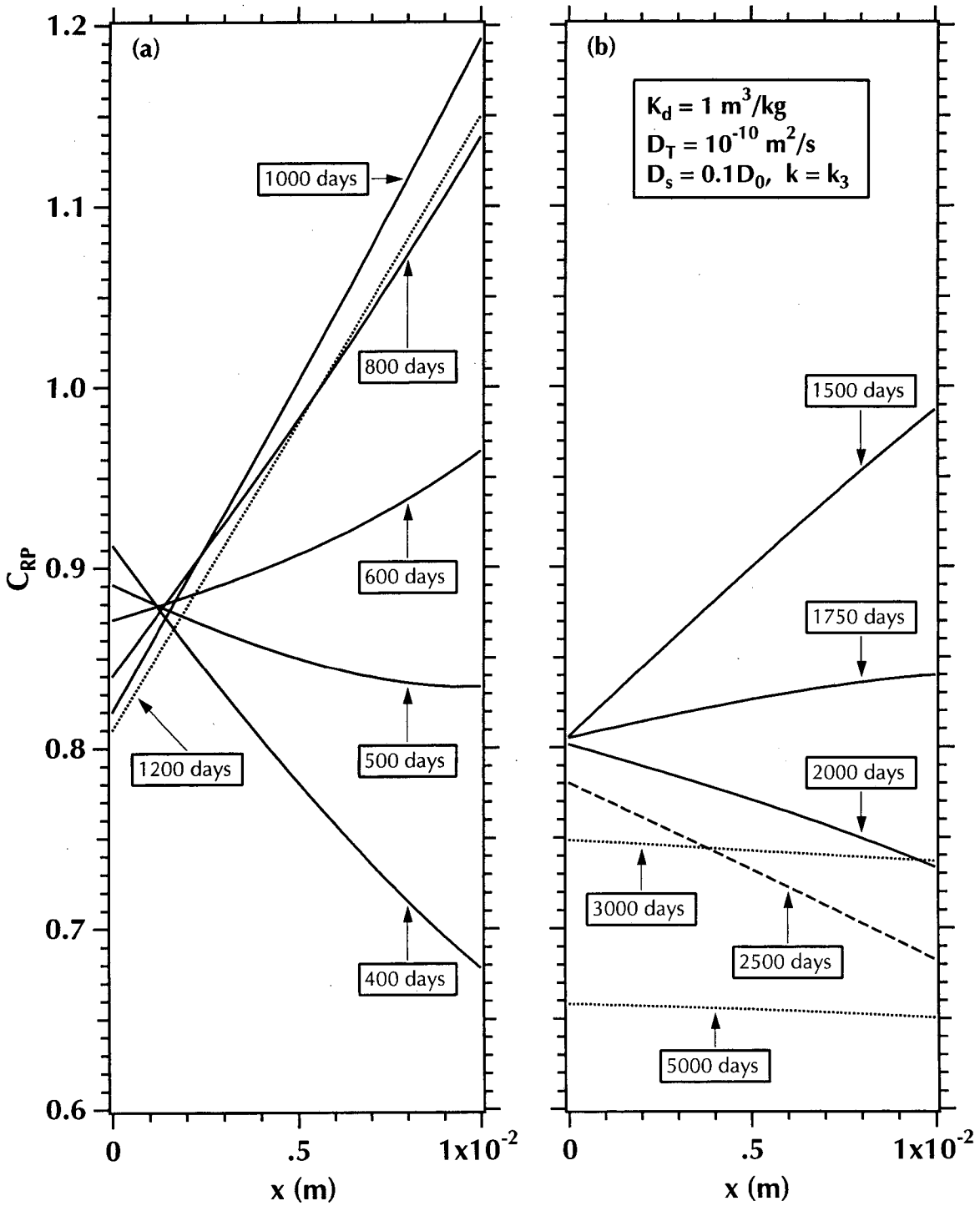

Figure 19. Spatial and temporal distribution of $C_{RP} = C(x)/C_{U0}$ in a PM sample with $L = 10^{-2}\ m$ under the conditions of the study for $k = k_3$ in Figure 17.

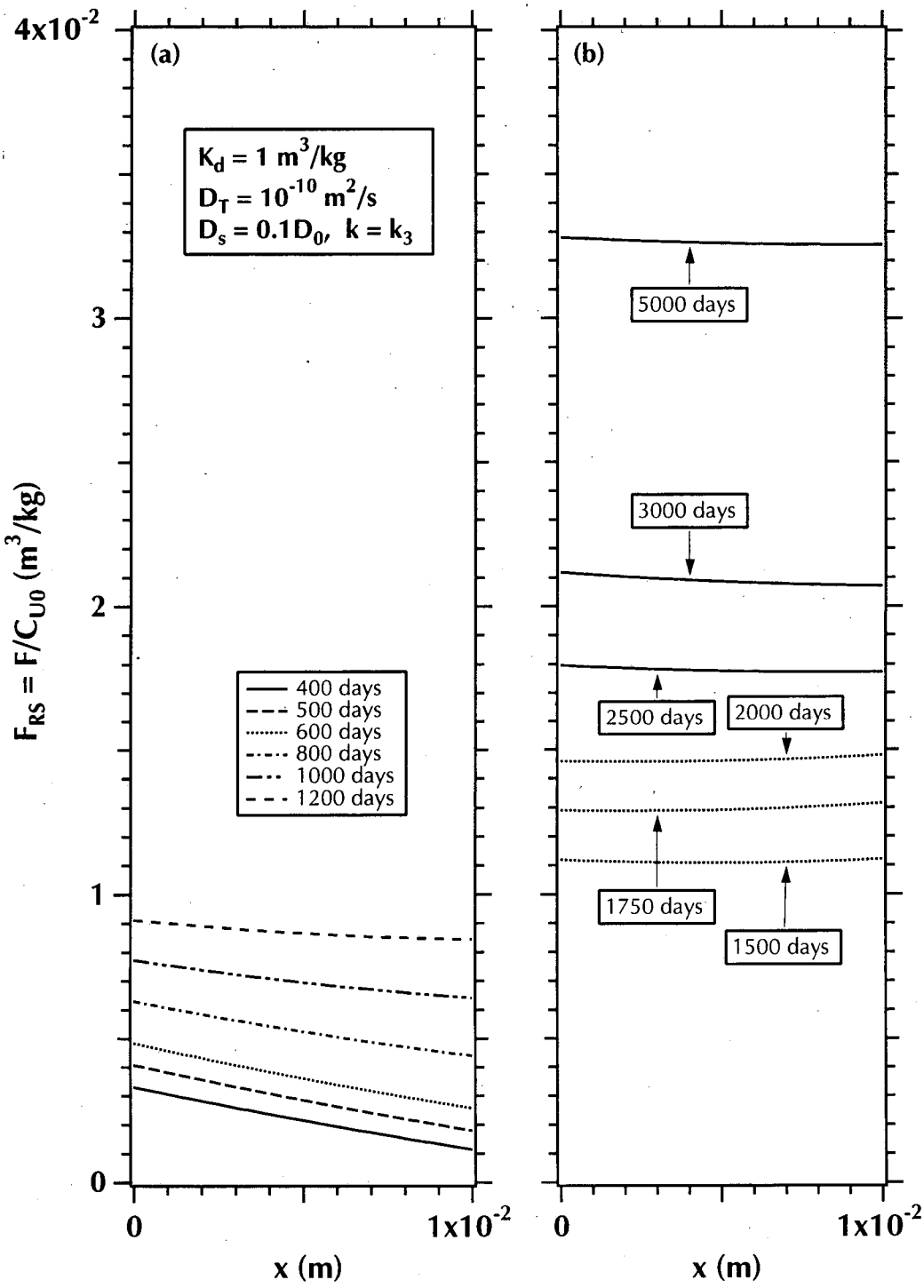

Figure 20. Spatial and temporal distribution of $F_{RS} = F/C_{U0}$ in a PM sample with $L = 10^{-2}$ m under the conditions of the study for $k = k_3$ in Figure 17.

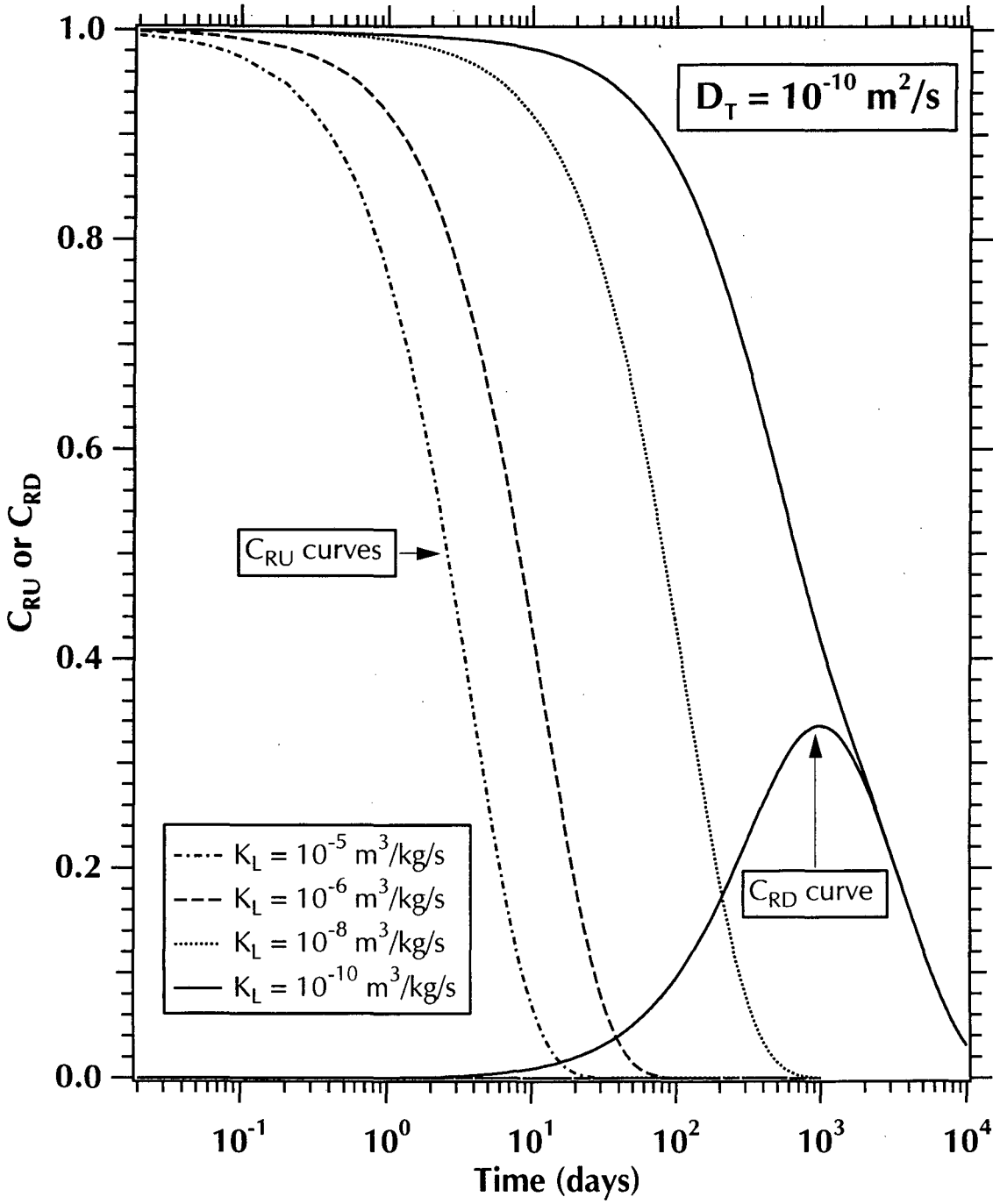

Figure 21. Effect of varying K_L on the C_{RU} and C_{RD} solutions under through-diffusion conditions with irreversible sorption.

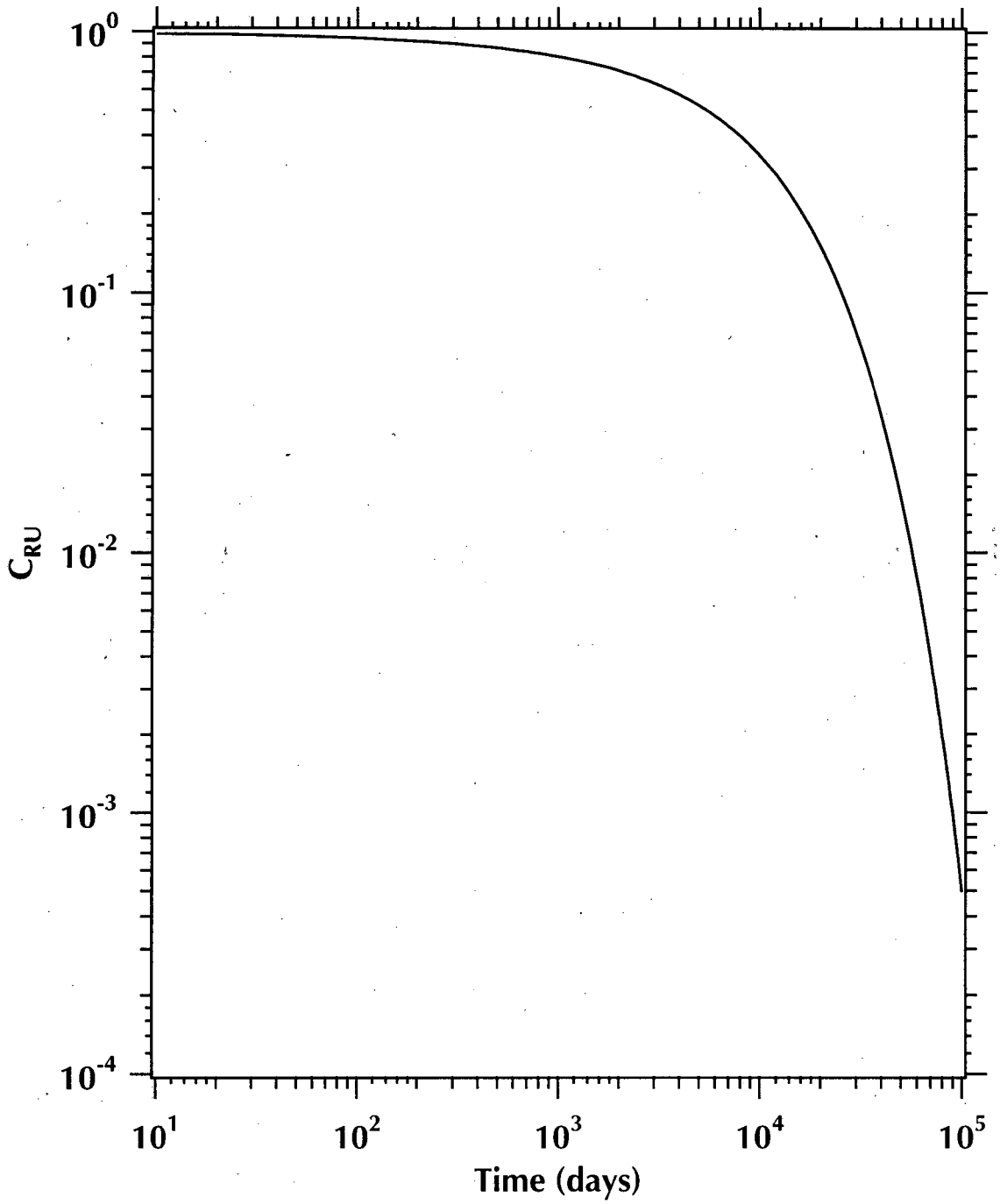

Figure 22. Scoping calculations of C_{RU} evolution over time in the example of the H-basin.

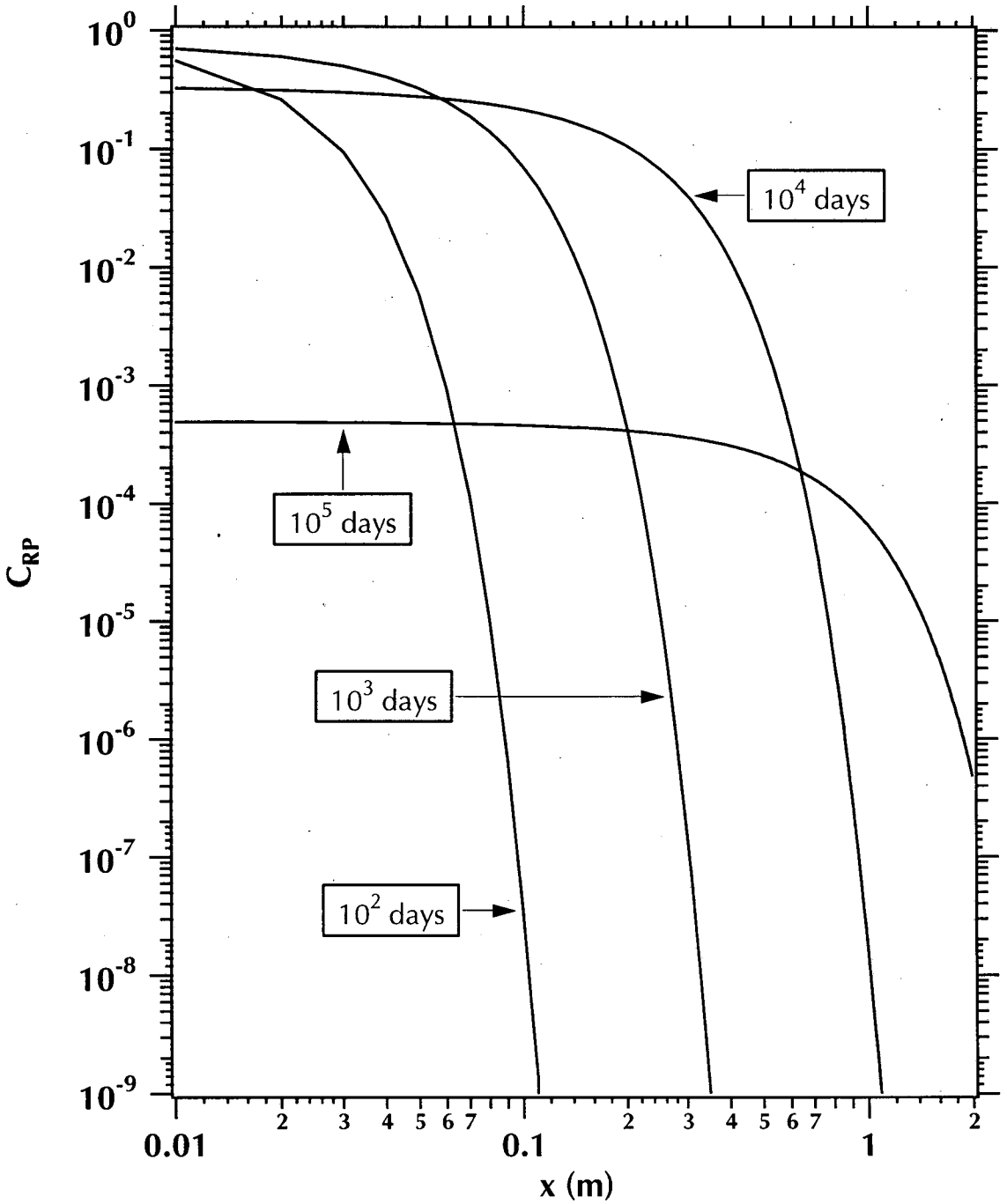

Figure 23. C_{RP} distribution over time in the PM of the H-basin example. Note that advection is neglected.

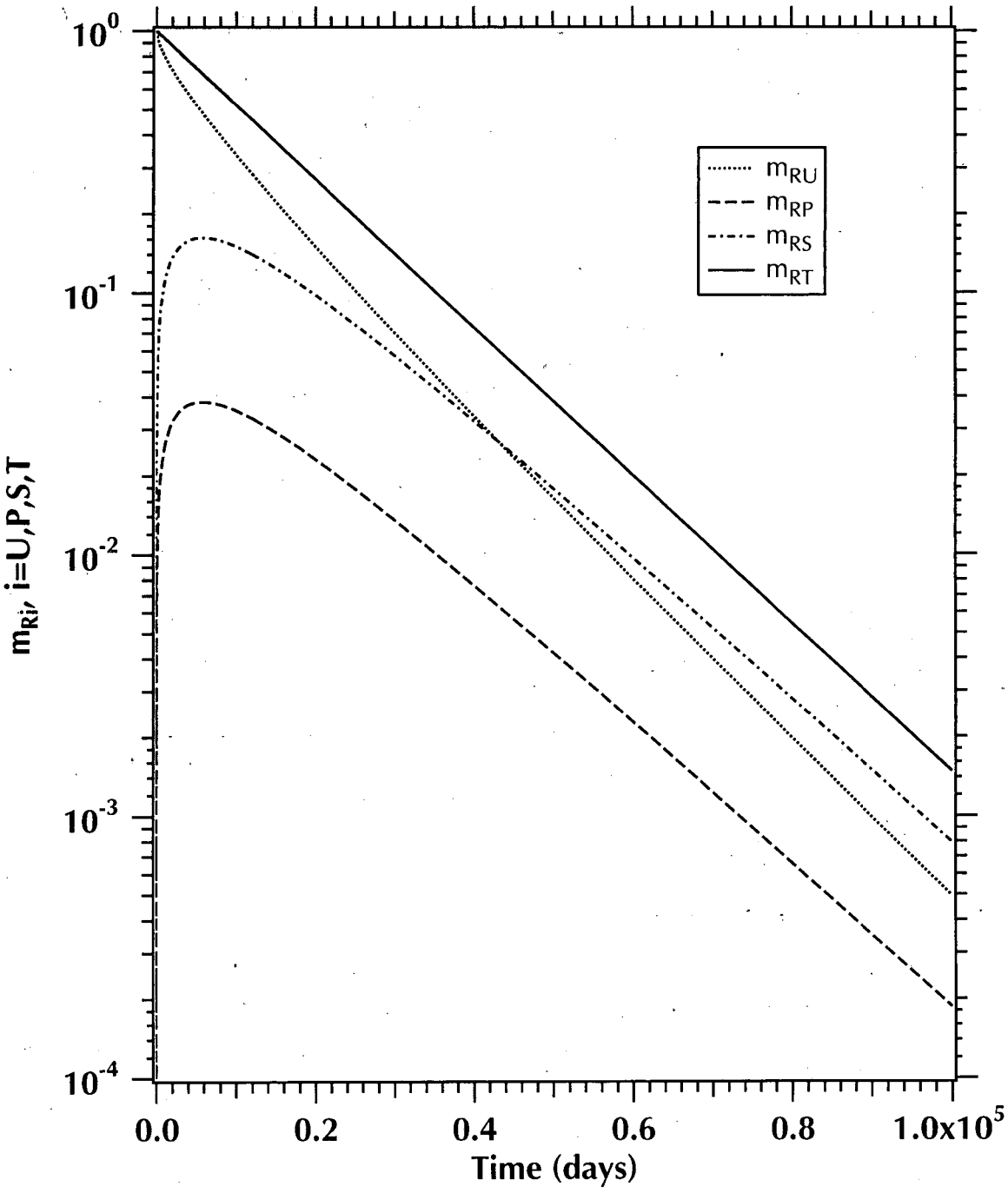

Figure 24. Relative masses of dissolved species in the various components of the H-basin system.

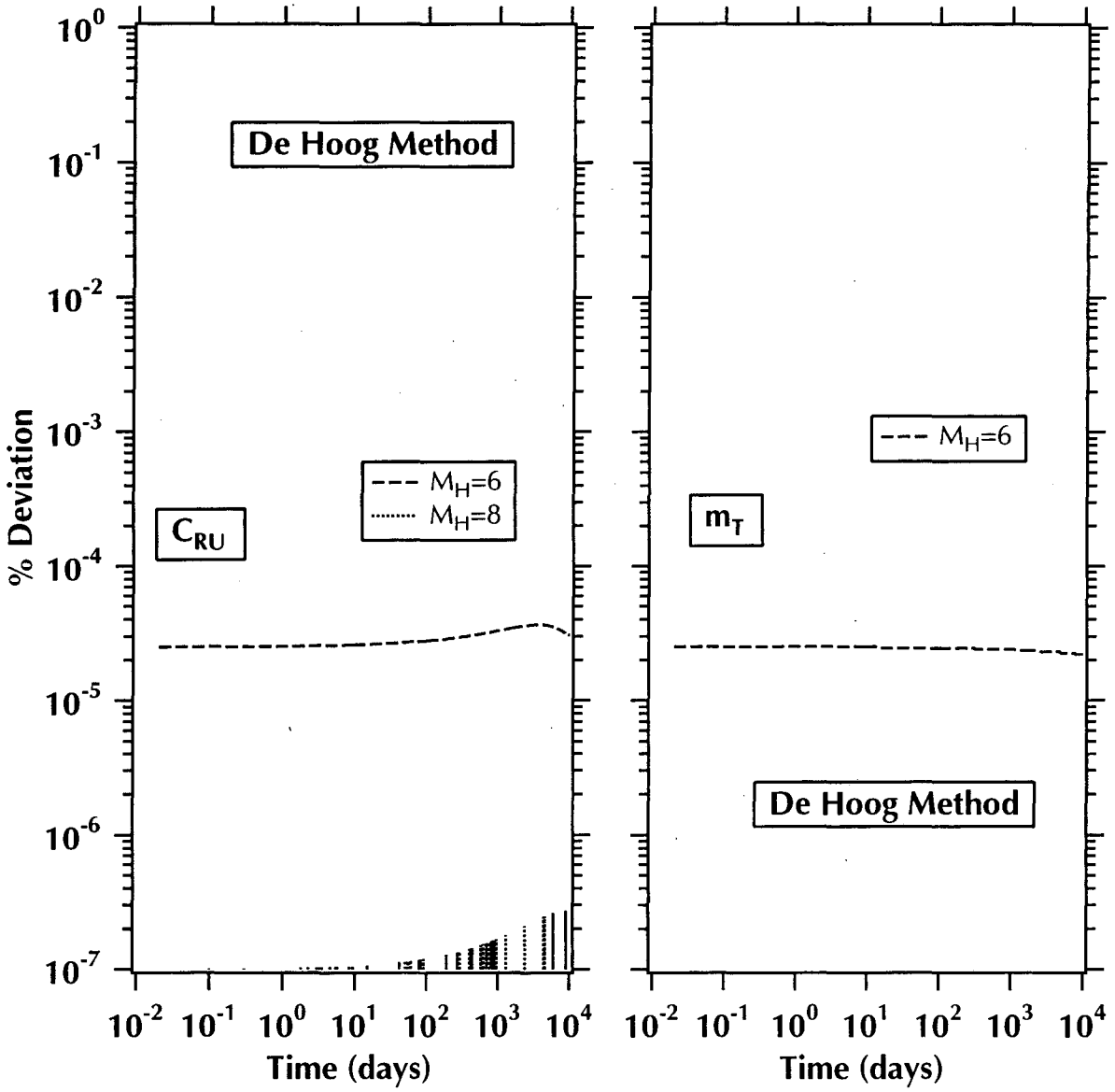

Figure 25. Effect of the M_H parameter in the De Hoog method ($6 \leq M_H \leq 22$) on the deviation (%) of the C_{RU} and m_T solutions from the standard solutions (obtained using the De Hoog method with $M_H = 20$). The curves for $M_H \geq 10$ exhibited deviations $\leq 10^{-7}$% and are not shown.

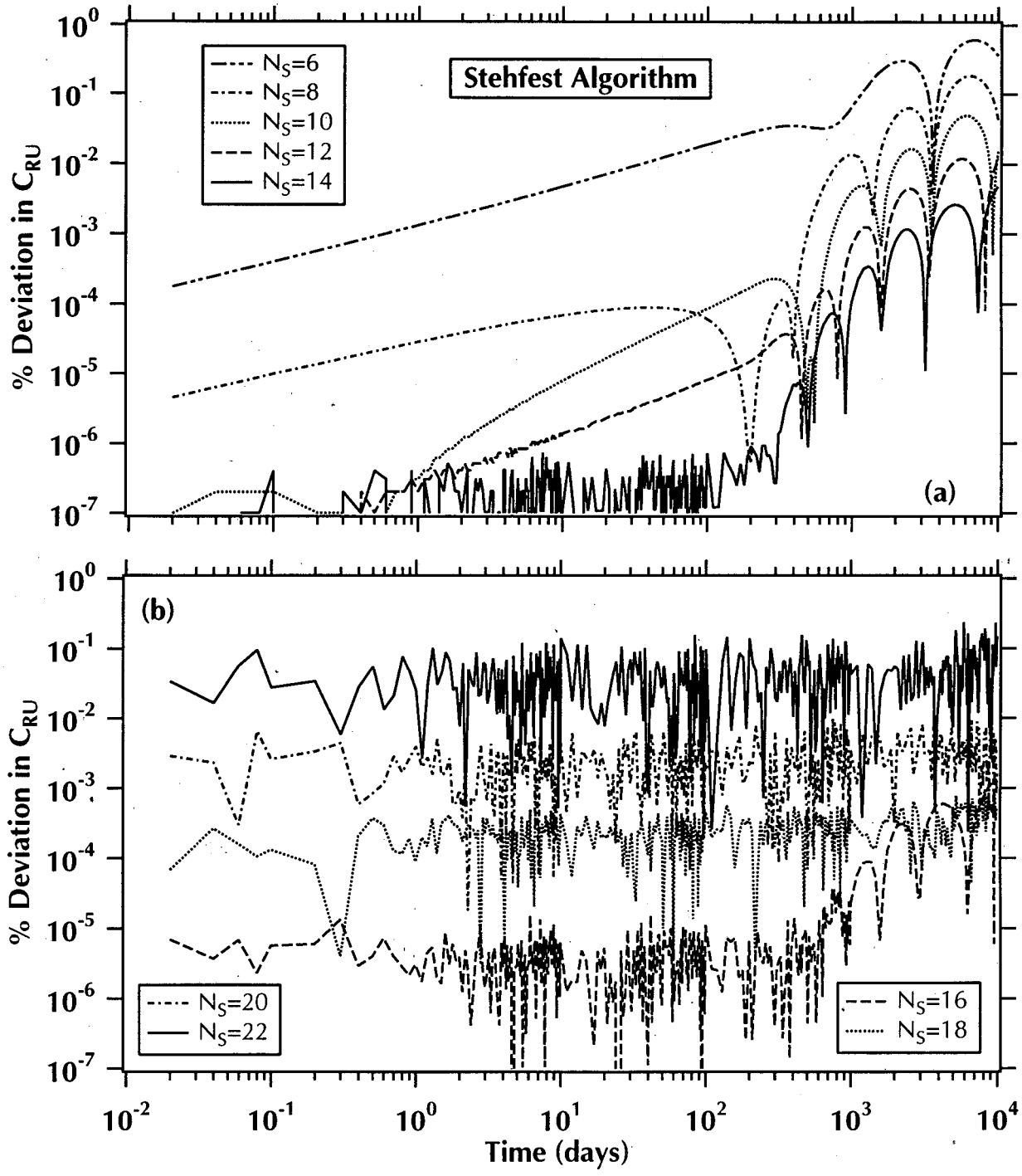

Figure 26. Effect of the N_S parameter in the Stehfest algorithm ($6 \leq N_S \leq 22$) on the deviation (%) of C_{RU} from the standard solution (De Hoog with $M_H = 20$).

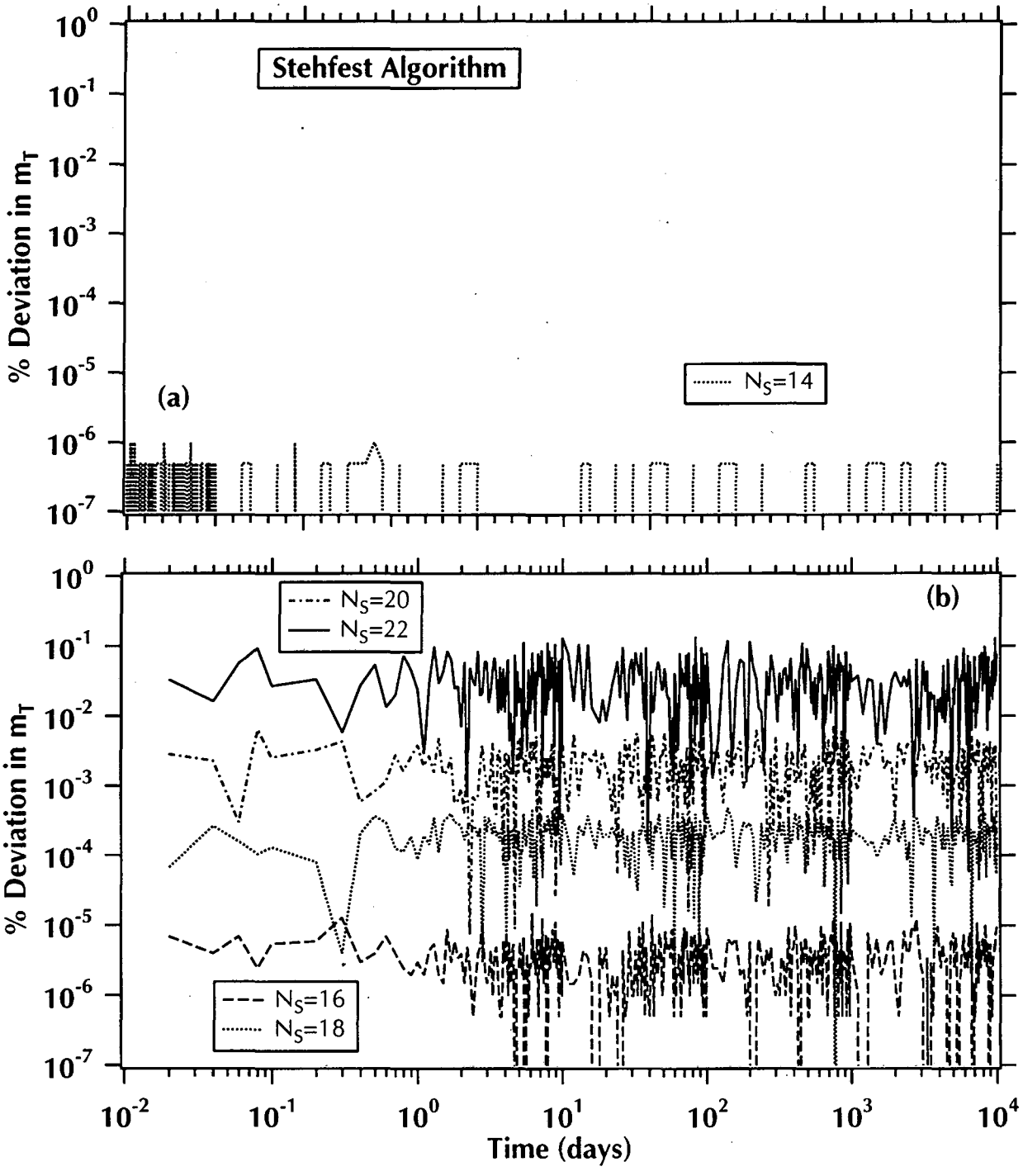

Figure 27. Effect of the N_S parameter in the Stehfest algorithm on the deviation (%) of m_T from the standard solution. Only the curves with deviations $\geq 10^{-7}$ % are shown.

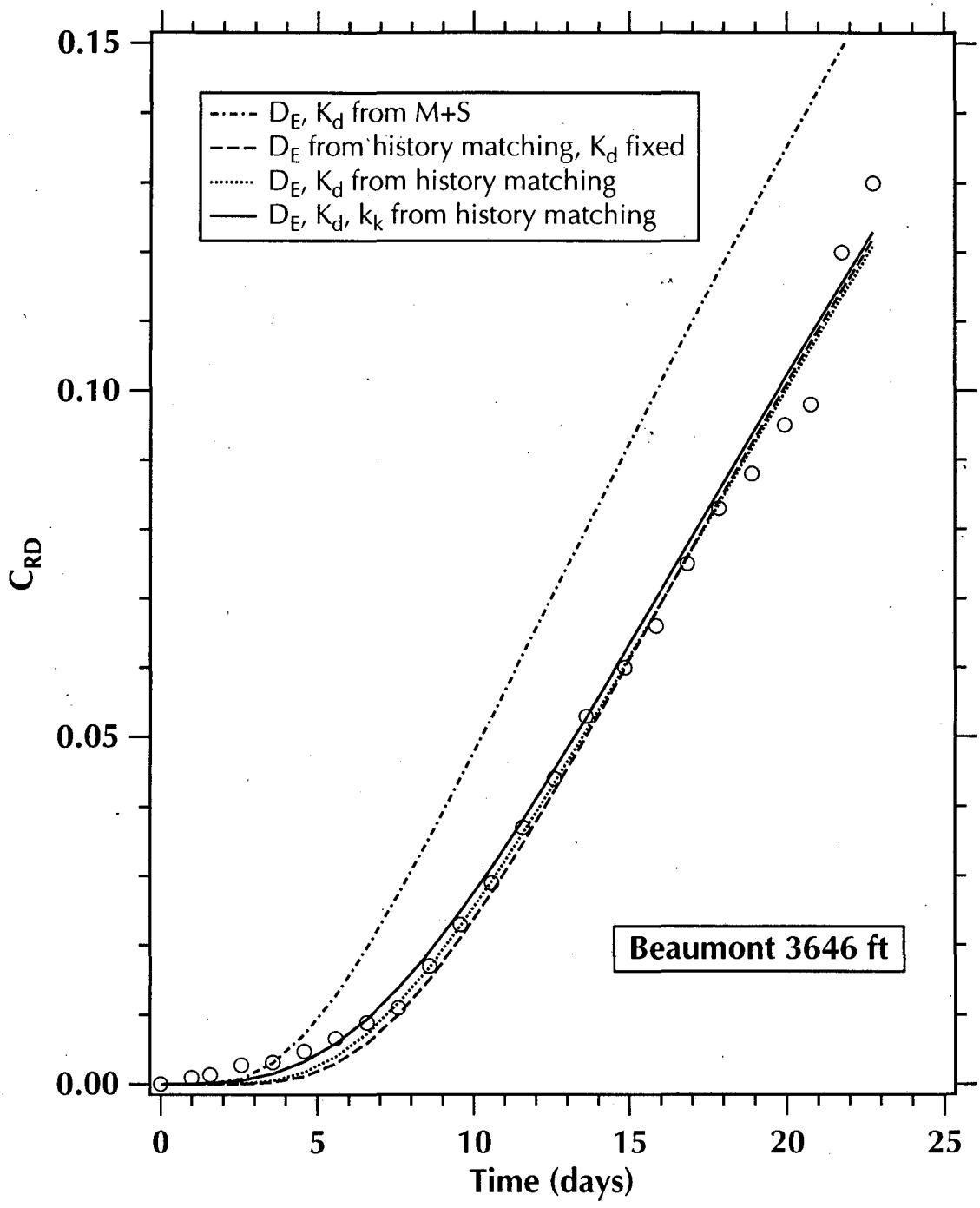

Figure 28. Comparison of measurements to SA1 predictions of C_{RD} with history-matched sorption/diffusion parameters in a 'Beaumont 3646 ft' sample [*McKinley and Swaminathan*, 1996].

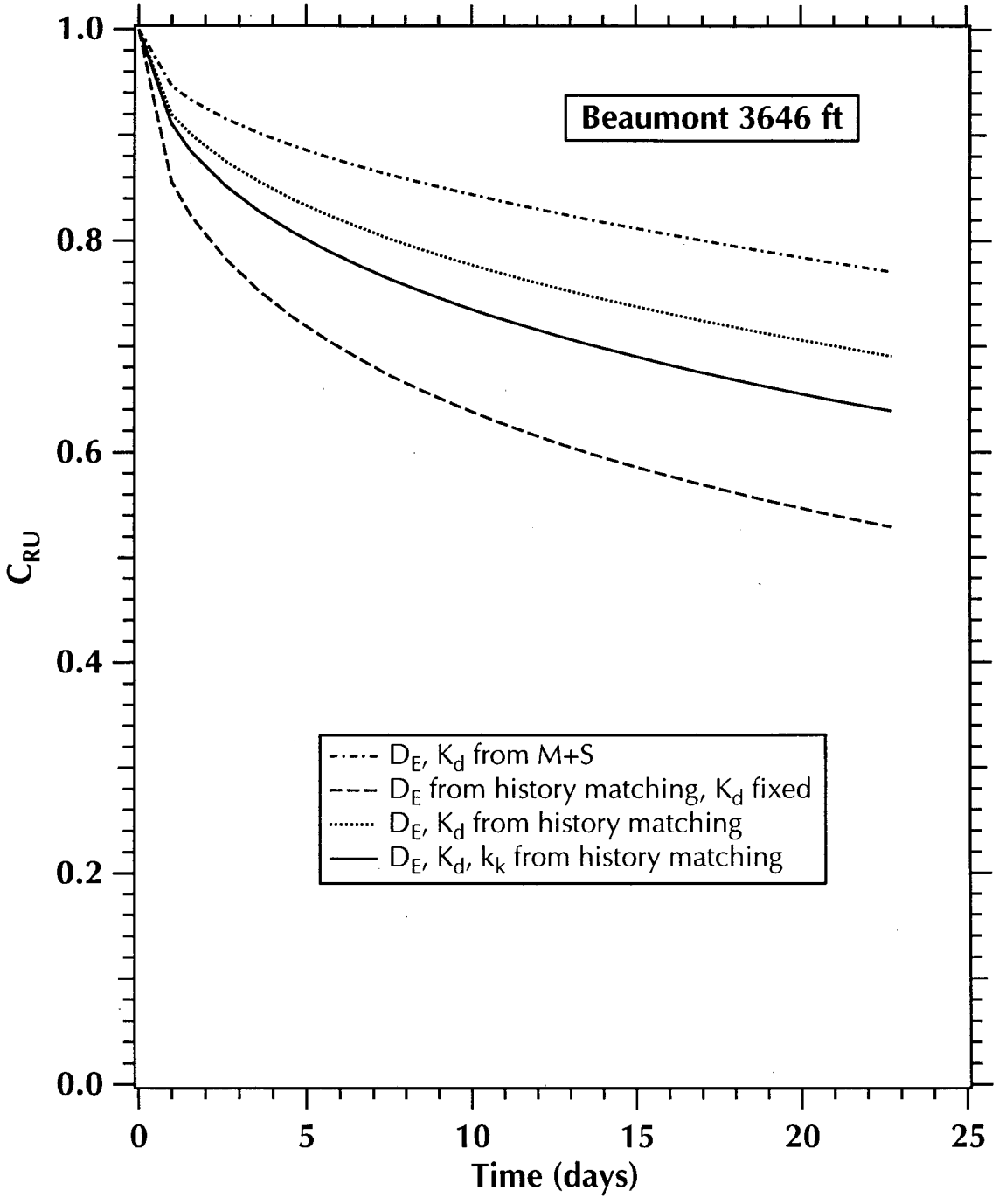

Figure 29. Predictions of C_{RU} corresponding to the C_{RD} curves in Figure 27.

Ernest Orlando Lawrence Berkeley National Laboratory
One Cyclotron Road | Berkeley, California 94720

Prepared for the U.S. Department of Energy under Contract No. DE-AC03-76SF00098